

From bypass transition to flow control and data-driven turbulence modeling: An input-output viewpoint

Mihailo R. Jovanović

Ming Hsieh Department of Electrical and Computer Engineering, University of Southern California, Los Angeles, California 90089, USA; email: mihailo@usc.edu

Xxxx. Xxx. Xxx. Xxx. 2021. AA:1–36

[https://doi.org/10.1146/\(\(please add article doi\)\)](https://doi.org/10.1146/((please add article doi)))

Copyright © 2021 by Annual Reviews.
All rights reserved

Keywords

input-output analysis, flow modeling and control, physics-aware data-driven modeling, stochastic dynamics, frequency responses, transition to turbulence, turbulent flows, convex optimization

Abstract

Transient growth and resolvent analyses are routinely used to assess non-asymptotic properties of fluid flows. In particular, resolvent analysis can be interpreted as a special case of viewing flow dynamics as an open system in which free-stream turbulence, surface roughness, and other irregularities provide sources of input forcing. We offer a comprehensive summary of the tools that can be employed to probe the dynamics of fluctuations around a laminar or turbulent base flow in the presence of such stochastic or deterministic input forcing and describe how input-output techniques enhance resolvent analysis. Specifically, physical insights that may remain hidden in the resolvent analysis are gained by detailed examination of input-output responses between spatially-localized body forces and selected linear combinations of state variables. This differentiating feature plays a key role in quantifying the importance of different mechanisms for bypass transition in wall-bounded shear flows and in explaining how turbulent jets generate noise. We highlight the utility of a stochastic framework, with white or colored inputs, in addressing a variety of open challenges including transition in complex fluids, flow control, and physics-aware data-driven turbulence modeling. Applications with time- or spatially-periodic base flows are discussed and future research directions are outlined.

Contents

1. INTRODUCTION	3
2. INPUT-OUTPUT VIEWPOINT: BEYOND RESOLVENT ANALYSIS	4
2.1. From evolution model to input-output representation	4
2.2. Amplification of deterministic inputs	7
2.3. Amplification of stochastic inputs	7
3. UNCOVERING MECHANISMS IN WALL-BOUNDED SHEAR FLOWS	12
3.1. Bypass transition in channel flows of Newtonian fluids	12
3.2. Early stages of transition to elastic turbulence: viscoelastic lift-up	15
3.3. Turbulent channel and pipe flows of Newtonian fluids	16
4. CONTROL OF TRANSITIONAL AND TURBULENT FLOWS	18
4.1. Controlling the onset of turbulence by streamwise traveling waves	20
4.2. Turbulent drag reduction by spanwise wall oscillations	22
5. PHYSICS-AWARE DATA-DRIVEN TURBULENCE MODELING	24
5.1. Completion of partially available channel flow statistics	25
6. DISCUSSION	29

1. INTRODUCTION

Hydrodynamic stability theory focuses on spectral analysis of the dynamical generator in the linearized Navier-Stokes (NS) equations while seeking the critical Reynolds number at which exponentially growing modes emerge (Schmid & Henningson 2001). Although in many flows predictions agree well with experiments, in wall-bounded shear flows both the critical Reynolds number and the spatial structure of the least-stable or unstable modes are at odds with experimental observations. A broader viewpoint, based on nonmodal analysis of the linearized NS equations, provides reconciliation with experiments and identifies mechanisms for the early stages of subcritical transition (Schmid 2007).

In the words of Trefethen & Embree (2005), the eigenvalue decomposition *gives a square matrix, or an operator, a personality*. However, this “personality test” is conclusive only for normal (i.e., unitarily diagonalizable) operators. For non-normal operators, it is the singular value decomposition (SVD) that offers a robust predictor of “personality” (Trefethen & Embree 2005). In wall-bounded shear flows, non-normality of the linearized dynamical operator introduces coupling of exponentially decaying modes which explains high sensitivity of the laminar flow (Schmid 2007). The high sensitivity degrades the accuracy of analytical and computational predictions that do not explicitly account for modeling imperfections. These are typically difficult to model and may arise from a variety of sources, including surface roughness, thermal fluctuations, and irregularities in the incoming stream.

The study of dynamical systems with input forcing has a rich history in several branches of electrical engineering including circuit theory, communications, signal processing, and control. In this, dynamical systems are decomposed into essential pieces and represented as interconnections of input-output “blocks”. This input-output viewpoint facilitates the analysis, design, and optimization of complex systems, since they can be viewed as simpler sub-systems placed in cascade, parallel, and feedback arrangements with one another. It also allows us to quantify the influence of modeling imperfections (e.g., background noise or experimental uncertainty that is unavoidable in physical systems) on quantities of interest.

In fluid mechanics, input-output analysis addresses the influence of deterministic as well as stochastic inputs on transient and asymptotic properties of fluid flows. It offers a complementary viewpoint to transient growth (Butler & Farrell 1992) and resolvent (Trefethen et al. 1993) analyses and brings in an appealing robustness interpretation. Specifically, additional insight about the dynamics is gained by carrying out SVD of the operator that maps excitation sources (i.e., inputs such as body forcing fluctuations) to the quantities of interest (i.e., outputs such as velocity fluctuations). In contrast to the resolvent, this operator is not necessarily a square object; it captures the effect of different inputs to particular physical quantities and thereby reveals finer physical aspects (Jovanović & Bamieh 2005). In wall-bounded shear flows, input-output analysis exposes large amplification of disturbances and high sensitivity of the laminar flow to uncertainty in the geometry or base velocity (Trefethen et al. 1993, Farrell & Ioannou 1993, Bamieh & Dahleh 2001, Jovanović 2004), and provides insights into structural features of turbulent flows (McKeon & Sharma 2010, Hwang & Cossu 2010a,b). Additional successful applications range from discovering mechanisms for transition to elastic turbulence in viscoelastic fluids (Hoda et al. 2008, 2009, Jovanović & Kumar 2011), to revealing how turbulent jets generate noise (Jeun et al. 2016), and explaining the origin of reattachment streaks in hypersonic flows (Dwivedi et al. 2019).

This review highlights the merits, effectiveness, and versatility of the input-output framework for modeling, analysis, and control of fluid flows. We offer a comprehensive summary of the tools that can be used to probe the dynamics of infinitesimal fluctuations

Time: t

Complex number:

$s = \sigma + i\omega$

Frequency: ω

Wavenumbers: \mathbf{k}

Dynamical generator:

$A_{\mathbf{k}}$

State-transition operator: $e^{A_{\mathbf{k}}t}$

Resolvent operator:

$(sI - A_{\mathbf{k}})^{-1}$

Input operator: $B_{\mathbf{k}}$

Output operator: $C_{\mathbf{k}}$

Impulse response:

$C_{\mathbf{k}} e^{A_{\mathbf{k}}t} B_{\mathbf{k}}$

Transfer function:

$C_{\mathbf{k}} (sI - A_{\mathbf{k}})^{-1} B_{\mathbf{k}}$

Frequency response:

$C_{\mathbf{k}} (i\omega I - A_{\mathbf{k}})^{-1} B_{\mathbf{k}}$

around a given laminar or turbulent base flow, and explain how the framework augments resolvent analysis (Trefethen et al. 1993). We illustrate how the componentwise input-output approach (Jovanović & Bamieh 2005) identifies key mechanisms for bypass transition in channel flows of Newtonian and viscoelastic fluids. We then describe how periodic base flow modifications, induced by streamwise traveling waves and spanwise wall-oscillations, can be designed to, respectively, control the onset of turbulence (Moarref & Jovanović 2010) and identify the optimal period of oscillation for turbulent drag reduction (Moarref & Jovanović 2012). The input-output framework is also well-suited for data-driven turbulence modeling; in contrast to physics-agnostic machine learning techniques, the tools from control theory and convex optimization allow for strategic use of data in order to capture second-order statistics of turbulent flows via first-principle models (Zare et al. 2017b, 2020).

2. INPUT-OUTPUT VIEWPOINT: BEYOND RESOLVENT ANALYSIS

We first review the tools that can be used to probe the dynamics of infinitesimal fluctuations around a given base flow. While this framework can be utilized in a variety of flow regimes and geometries, we resort to a channel flow with homogeneous wall-parallel directions to illustrate the key concepts; see **Figure 1(a)**. Even in this simple setup a variety of non-trivial fundamental questions can be addressed by employing an input-output viewpoint, including transition in complex fluids, flow control, and data-driven turbulence modeling.

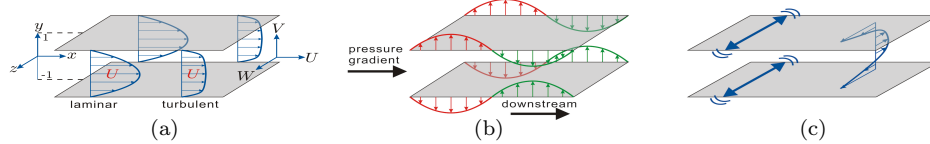


Figure 1

A pressure-driven channel flow (a) between two parallel infinite walls with base flow $(U(y), 0, 0)$, inhomogeneous wall-normal (y), and homogeneous streamwise and spanwise (x, z) directions; (b) subject to blowing and suction along the walls; and (c) subject to spanwise wall-oscillations.

2.1. From evolution model to input-output representation

The linearized NS equations govern the dynamics of infinitesimal fluctuations around a given base flow. Fluctuations can arise from a variety of sources, including surface roughness, imperfections in the incoming stream, acoustics, vibrations, particles, and impurities. In turbulent flows, nonlinear interactions between different length scales can also provide forcing that sustains fluctuations. The linearized NS equations, with an input forcing $\mathbf{d}_{\mathbf{k}}(t)$ and an output of interest $\boldsymbol{\xi}_{\mathbf{k}}(t)$, can be brought to an evolution form,

$$\begin{aligned} \frac{d\boldsymbol{\psi}_{\mathbf{k}}(t)}{dt} &= A_{\mathbf{k}} \boldsymbol{\psi}_{\mathbf{k}}(t) + B_{\mathbf{k}} \mathbf{d}_{\mathbf{k}}(t), \\ \boldsymbol{\xi}_{\mathbf{k}}(t) &= C_{\mathbf{k}} \boldsymbol{\psi}_{\mathbf{k}}(t), \end{aligned} \tag{1}$$

where $\boldsymbol{\psi}_{\mathbf{k}}(t)$ is the state and \mathbf{k} is the vector of wavenumbers. The operator $A_{\mathbf{k}}$ characterizes dynamical interactions between the states, $B_{\mathbf{k}}$ specifies the way the input $\mathbf{d}_{\mathbf{k}}(t)$ enters into the dynamics, and $C_{\mathbf{k}}$ maps the state $\boldsymbol{\psi}_{\mathbf{k}}(t)$ to the output $\boldsymbol{\xi}_{\mathbf{k}}(t)$. Equation 1 is a standard state-space model in the controls literature, and it provides a convenient starting point for modal and nonmodal analysis, system identification, turbulence modeling, and flow control.

Evolution Model 1:

A 1st order (in time) differential equation governs the evolution of the state $\boldsymbol{\psi}_{\mathbf{k}}(t)$ and a static-in-time output equation relates $\boldsymbol{\psi}_{\mathbf{k}}(t)$ to the output $\boldsymbol{\xi}_{\mathbf{k}}(t) = C_{\mathbf{k}} \boldsymbol{\psi}_{\mathbf{k}}(t)$. Apart from the boundary conditions, no additional constraints are imposed on $\boldsymbol{\psi}_{\mathbf{k}}(t)$.

For a pressure-driven channel flow of an incompressible Newtonian fluid, the base flow $\bar{\mathbf{u}}$ is either given by the laminar parabolic profile (Poiseuille flow) or the turbulent mean velocity. In both cases, the flow is fully-developed and $\bar{\mathbf{u}}$ only depends on the wall-normal distance y , $\bar{\mathbf{u}} = (U(y), 0, 0)$. Thus, the linearized NS equations are translationally-invariant in wall-parallel directions and in time and fluctuations can be decomposed in terms of the normal modes in x and z as $\psi(x, y, z, t) = \psi_{\mathbf{k}}(y, t) e^{i(k_x x + k_z z)}$. Here, $\mathbf{k} := (k_x, k_z)$ denotes the vector of wall-parallel wavenumbers and $A_{\mathbf{k}}$ is the Orr-Sommerfeld/Squire operator (Schmid & Henningson 2001). In addition to \mathbf{k} , System 1 is parameterized by the base flow $\bar{\mathbf{u}}$ and the Reynolds number Re . For any (\mathbf{k}, t) , the state $\psi_{\mathbf{k}}(t)$, input $\mathbf{d}_{\mathbf{k}}(t)$, and output $\xi_{\mathbf{k}}(t)$ are functions of y but, for notational convenience, we suppress this dependence.

Derivation of Equation 1. The linearized model is obtained by expressing the flow as the sum of the base and fluctuation components and by neglecting the quadratic fluctuation terms. In incompressible flows of Newtonian fluids, the velocity obeys a continuity equation and a Poisson equation for the pressure p is obtained by applying the divergence operator to the linearized NS equations. The Orr-Sommerfeld equation is obtained by acting with the Laplacian Δ on the wall-normal velocity equation and using the expression for Δp to eliminate p . The Squire equation is obtained by taking the curl of the linearized NS equations. This yields an evolution model, in the form of two PDEs, for the wall-normal velocity and vorticity (Kim et al. 1987), $\psi := (v, \eta)$. All other velocity and vorticity components can be expressed in terms of (v, η) via kinematic relations (Jovanović & Bamieh 2005).

Standard stability analysis of a laminar Poiseuille flow predicts modal instability for $Re = 5772$. The discrepancy with experiments, in which transition occurs for $Re \approx 1000$, can be explained using nonmodal analysis (Schmid 2007) which reveals significant transient growth of fluctuations (Gustavsson 1991, Butler & Farrell 1992) and strong amplification of disturbances (Trefethen et al. 1993, Farrell & Ioannou 1993, Bamieh & Dahleh 2001).

2.1.1. Resolvent, transfer function, impulse and frequency response operators. While the governing equations and geometry determine the dynamical generator $A_{\mathbf{k}}$, there is flexibility in selecting the operators $B_{\mathbf{k}}$ and $C_{\mathbf{k}}$ and different choices can reveal different aspects of flow physics (Jovanović & Bamieh 2005). All of these operators play a role in the response of System 1 which arises from the initial condition $\psi_{\mathbf{k}}(0)$ and the exogenous input $\mathbf{d}_{\mathbf{k}}(t)$,

$$\xi_{\mathbf{k}}(t) = \underbrace{C_{\mathbf{k}} e^{A_{\mathbf{k}} t} \psi_{\mathbf{k}}(0)}_{\text{natural response}} + \underbrace{\int_0^t C_{\mathbf{k}} e^{A_{\mathbf{k}}(t-\tau)} B_{\mathbf{k}} \mathbf{d}_{\mathbf{k}}(\tau) d\tau}_{\text{forced response}}, \quad 2.$$

where $e^{A_{\mathbf{k}} t}$ is the *state-transition operator* associated with $A_{\mathbf{k}}$. The Laplace transform can be utilized to rewrite Equation 2 as,

$$\hat{\xi}_{\mathbf{k}}(s) = \underbrace{C_{\mathbf{k}} (sI - A_{\mathbf{k}})^{-1} \psi_{\mathbf{k}}(0)}_{\text{natural response}} + \underbrace{C_{\mathbf{k}} (sI - A_{\mathbf{k}})^{-1} B_{\mathbf{k}} \hat{\mathbf{d}}_{\mathbf{k}}(s)}_{\text{forced response}}, \quad 3.$$

where s is the complex number, I is the identity operator, $\hat{\xi}_{\mathbf{k}}(s)$ is the Laplace transform of $\xi_{\mathbf{k}}(t)$, and $(sI - A_{\mathbf{k}})^{-1}$ is the *resolvent operator*. Equations 2 and 3 determine responses of System 1 and provide the basis for quantifying important dynamical features of the linearized flow equations. As the blue terms demonstrate, the natural (i.e., unforced) responses are characterized by the state-transition $e^{A_{\mathbf{k}} t}$ and resolvent $(sI - A_{\mathbf{k}})^{-1}$ operators. On the other hand, the forced response is obtained by convolving an input $\mathbf{d}_{\mathbf{k}}(t)$ with the *impulse*

response operator $T_{\mathbf{k}}(t)$; equivalently, the *transfer function* $T_{\mathbf{k}}(s)$ specifies an input-output mapping in the complex domain, i.e., $\hat{\xi}_{\mathbf{k}}(s) = T_{\mathbf{k}}(s) \hat{\mathbf{d}}_{\mathbf{k}}(s)$, where

$$\begin{array}{ccc} \text{impulse response} & \xrightarrow{\text{Laplace transform}} & \text{transfer function} \\ T_{\mathbf{k}}(t) := C_{\mathbf{k}} e^{A_{\mathbf{k}} t} B_{\mathbf{k}} & & T_{\mathbf{k}}(s) := C_{\mathbf{k}} (sI - A_{\mathbf{k}})^{-1} B_{\mathbf{k}}. \end{array}$$

For flows over perfectly smooth walls and in noise-free environments, study of natural responses aids in understanding the fundamental fluid mechanics. Specifically, the eigenvalue decomposition of $A_{\mathbf{k}}$ and the singular value decomposition of $e^{A_{\mathbf{k}} t}$, respectively, offer insights into modal and nonmodal aspects of the flow (Schmid 2007). While such insights are valuable, engineering flows seldom exist in isolation and understanding the forced responses is equally important. In particular, input-output analysis examines forced responses with the objective of quantifying amplification of disturbances and impact of modeling imperfections on fluctuations' dynamics. In contrast to natural responses, study of forced responses requires specifying how disturbances enter into System 1, through the operator $B_{\mathbf{k}}$.

In the special case when the input excites all degrees of freedom equally and the output is the entire state, $B_{\mathbf{k}}$ and $C_{\mathbf{k}}$ are the identity operators and the resolvent completely determines the transfer function. However, it is often of interest to confine the inputs to certain spatial regions and to examine outputs that are given by a linear combination of certain state variables. In such cases, the transfer function is determined by a ‘‘compressed resolvent’’ and its analysis can uncover important dynamical aspects that may be obscured by only paying attention to the ‘‘standard resolvent’’. This distinction played a key role in understanding how turbulent jets generate noise. Jeun et al. (2016) utilized ‘‘compressed resolvent’’ analysis by restricting inputs to the vicinity of the jet turbulence and selecting far-field pressure as the output. In contrast to a standard resolvent analysis, which provides links to jet hydrodynamics but does not explain noise generation (Garnaud et al. 2013), this approach identifies acoustic sources to be wavepackets that are in excellent agreement with experiments (Jordan & Colonius 2013) and reveals mechanisms for noise generation.

Singular Value Decomposition. In transient growth analysis, SVD identifies spatial structure of initial conditions that maximize energy at a given time. SVD also provides the tool for quantifying responses to unsteady deterministic as well as stochastic inputs $\mathbf{d}_{\mathbf{k}}(t)$ that neither grow nor decay in time (on average). This allows us to set $s = i\omega$, and the frequency response $T_{\mathbf{k}}(i\omega)$ is obtained by evaluating the transfer function $T_{\mathbf{k}}(s)$ along the imaginary axis; see the sidebar FREQUENCY RESPONSE OPERATOR.

SVD of $T_{\mathbf{k}}(i\omega)$ identifies fundamental input-output features across (\mathbf{k}, ω) ,

$$\hat{\xi}_{\mathbf{k}}(i\omega) = T_{\mathbf{k}}(i\omega) \hat{\mathbf{d}}_{\mathbf{k}}(i\omega) = \sum_{j=1}^{\infty} \sigma_{\mathbf{k},j}(\omega) \hat{\mathbf{u}}_{\mathbf{k},j}(\omega) \langle \hat{\mathbf{v}}_{\mathbf{k},j}(\omega), \hat{\mathbf{d}}_{\mathbf{k}}(i\omega) \rangle. \quad 4a.$$

The left and right singular functions, $\hat{\mathbf{v}}_{\mathbf{k},j}(\omega)$ and $\hat{\mathbf{u}}_{\mathbf{k},j}(\omega)$, provide orthonormal bases of the input and output spaces, the singular value $\sigma_{\mathbf{k},j}(\omega)$ determines the corresponding amplification, and $\langle \cdot, \cdot \rangle$ is the inner product. SVD requires computation of the adjoint $T_{\mathbf{k}}^{\dagger}(i\omega)$,

$$\langle T_{\mathbf{k}}^{\dagger}(i\omega) \hat{\xi}_{\mathbf{k}}(i\omega), \hat{\mathbf{d}}_{\mathbf{k}}(i\omega) \rangle = \langle \hat{\xi}_{\mathbf{k}}(i\omega), T_{\mathbf{k}}(i\omega) \hat{\mathbf{d}}_{\mathbf{k}}(i\omega) \rangle, \quad 4b.$$

and the eigenvalue decomposition of TT^{\dagger} and $T^{\dagger}T$, $T_{\mathbf{k}}(i\omega)T_{\mathbf{k}}^{\dagger}(i\omega)\hat{\mathbf{u}}_{\mathbf{k},j}(\omega) = \sigma_{\mathbf{k},j}^2(\omega)\hat{\mathbf{u}}_{\mathbf{k},j}(\omega)$, $T_{\mathbf{k}}^{\dagger}(i\omega)T_{\mathbf{k}}(i\omega)\hat{\mathbf{v}}_{\mathbf{k},j}(\omega) = \sigma_{\mathbf{k},j}^2(\omega)\hat{\mathbf{v}}_{\mathbf{k},j}(\omega)$. Unless noted otherwise, the L_2 inner product $\langle \cdot, \cdot \rangle$, which induces energy norm, is taken over inhomogeneous spatial directions in Equation 4.

Inner product: $\langle \cdot, \cdot \rangle$

Norm: $\| \cdot \|$

Tensor product:

$[\mathbf{u} \otimes \mathbf{v}] \mathbf{w} := \mathbf{u} \langle \mathbf{v}, \mathbf{w} \rangle$

Square-integrable

function space: L_2

Complex-conjugate

transpose: $(\cdot)^*$

Adjoint: $(\cdot)^{\dagger}$

Expectation

operator: $\mathbf{E}(\cdot)$

Supremum: sup

Set of integers: \mathbb{Z}

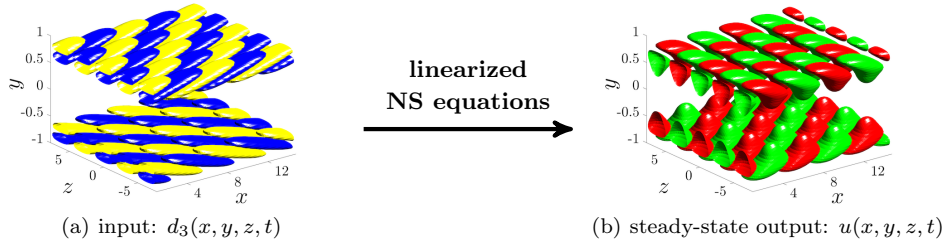


Figure 2

In linearly stable channel flows, the steady-state response of the linearized NS equations to a harmonic input in (x, z, t) , $\hat{\mathbf{d}}_{\mathbf{k}}(y, i\omega) e^{i(k_x x + k_z z + \omega t)}$, is determined by $\hat{\xi}_{\mathbf{k}}(y, i\omega) e^{i(k_x x + k_z z + \omega t)}$, where $\hat{\xi}_{\mathbf{k}}(y, i\omega) = [T_{\mathbf{k}}(i\omega)\hat{\mathbf{d}}_{\mathbf{k}}(\cdot, i\omega)](y)$. Spatial structures of (a) spanwise forcing fluctuations; and (b) resulting streamwise velocity fluctuations at one time instant in Poiseuille flow with $Re = 2000$ for 4 combinations of $(k_x, k_z, \omega) = (1, \pm 1, -0.385); (-1, \pm 1, 0.385)$.

2.2. Amplification of deterministic inputs

For a harmonic input $\mathbf{d}_{\mathbf{k}}(t) = \hat{\mathbf{d}}_{\mathbf{k}}(i\omega)e^{i\omega t}$ with $\hat{\mathbf{d}}_{\mathbf{k}}(i\omega) = \hat{\mathbf{v}}_{\mathbf{k},j}(\omega)$, where $\hat{\mathbf{v}}_{\mathbf{k},j}(\omega)$ is the j th left singular function of $T_{\mathbf{k}}(i\omega)$, the steady-state output $\xi_{\mathbf{k}}(t) = \hat{\xi}_{\mathbf{k}}(i\omega)e^{i\omega t}$ of System 1 is in the direction of the j th right singular function, $\hat{\xi}_{\mathbf{k}}(i\omega) = \sigma_{\mathbf{k},j}(\omega)\hat{\mathbf{u}}_{\mathbf{k},j}(\omega)$, and its energy is given by $\|\hat{\xi}_{\mathbf{k}}(i\omega)\|_2^2 := \langle \hat{\xi}_{\mathbf{k}}(i\omega), \hat{\xi}_{\mathbf{k}}(i\omega) \rangle = \sigma_{\mathbf{k},j}^2(\omega)$. The principal singular value, $\sigma_{\mathbf{k},1}(\omega) := \sigma_{\max}(T_{\mathbf{k}}(i\omega))$, determines the largest amplification at any (\mathbf{k}, ω) and the smallest upper bound over ω determines the H_{∞} norm of System 1 (Zhou et al. 1996), $G_{\mathbf{k}} := \sup_{\omega} \sigma_{\mathbf{k},1}^2(\omega)$. This measure of input-output amplification has several appealing interpretations for any \mathbf{k} .

- The H_{∞} norm represents the worst-case amplification of harmonic (in homogeneous directions and in time) deterministic (in inhomogeneous directions) inputs. This worst-case input-output gain is obtained by maximizing over spatial profiles (largest singular value of $T_{\mathbf{k}}$) and temporal frequency (supremum over ω); see **Figure 3(a)**.
- The H_{∞} norm determines the induced gain from finite energy inputs to outputs, $G_{\mathbf{k}} = \sup_{E_{\mathbf{k}}^{\text{in}} \leq 1} (E_{\mathbf{k}}^{\text{out}}/E_{\mathbf{k}}^{\text{in}})$, where $E_{\mathbf{k}}^{\text{in}}$ and $E_{\mathbf{k}}^{\text{out}}$ denote the \mathbf{k} -parameterized energy of input and output, e.g., $E_{\mathbf{k}}^{\text{in}} := \int_0^{\infty} \|\mathbf{d}_{\mathbf{k}}(t)\|_2^2 dt$, with $\|\mathbf{d}_{\mathbf{k}}(t)\|_2^2 = \langle \mathbf{d}_{\mathbf{k}}(t), \mathbf{d}_{\mathbf{k}}(t) \rangle$. For a unit-energy input $\mathbf{d}_{\mathbf{k}}(t)$ to stable System 1, $G_{\mathbf{k}}$ quantifies the largest possible energy of the output $\xi_{\mathbf{k}}(t)$ across the spatial wavenumber \mathbf{k} .
- The H_{∞} norm quantifies robustness to modeling imperfections; see **Figure 3(b)**.

2.3. Amplification of stochastic inputs

A common criticism of transient growth and resolvent analyses is difficulty of implementing the worst-case initial conditions or inputs in the lab. An alternative approach introduces a random excitation to the NS equations that can account for background noise. It identifies almost identical dominant flow structures and opens the door to turbulence modeling.

Control-theoretic tools can be utilized to exploit the structure of the linearized Model 1, avoid costly stochastic simulations, and offer insight into amplification mechanisms. For 20 realizations of persistent channel-wide temporally and spatially uncorrelated stochastic input $\mathbf{d}_{\mathbf{k}}(t)$ to Equation 1, **Figure 4** shows the variance of the velocity fluctuation vector $\mathbf{v}_{\mathbf{k}}(t) := (u_{\mathbf{k}}(t), v_{\mathbf{k}}(t), w_{\mathbf{k}}(t))$ in Poiseuille flow with $Re = 2000$. Although individual simulations display different responses, their average (marked by a thick black line) reaches the steady-state limit. In the absence of modal instability, viscosity asymptotically dissipates natural responses but a persistent excitation source maintains fluctuations for all times.

FREQUENCY RESPONSE OPERATOR

Time-invariant systems. The natural response of a stable Linear Time-Invariant (LTI) System 1 asymptotically decays to zero. The frequency response operator determines the steady-state response to harmonic inputs with frequency ω and is obtained by evaluating the transfer function along the imaginary axis,

$$T_{\mathbf{k}}(i\omega) := T_{\mathbf{k}}(s) \Big|_{s=i\omega} = C_{\mathbf{k}}(i\omega I - A_{\mathbf{k}})^{-1} B_{\mathbf{k}}. \quad \text{FR.}$$

For $\mathbf{d}_{\mathbf{k}}(t) = \hat{\mathbf{d}}_{\mathbf{k}}(i\omega)e^{i\omega t}$, the steady-state response of a stable System 1 is harmonic with the same frequency but with different amplitude and phase, i.e., $\boldsymbol{\xi}_{\mathbf{k}}(t) = \hat{\boldsymbol{\xi}}_{\mathbf{k}}(i\omega)e^{i\omega t}$. The frequency response $T_{\mathbf{k}}(i\omega)$ is an operator (in inhomogeneous spatial directions) that maps a spatial input profile $\hat{\mathbf{d}}_{\mathbf{k}}(i\omega)$ into the output $\hat{\boldsymbol{\xi}}_{\mathbf{k}}(i\omega)$, $\hat{\boldsymbol{\xi}}_{\mathbf{k}}(i\omega) = T_{\mathbf{k}}(i\omega)\hat{\mathbf{d}}_{\mathbf{k}}(i\omega)$, thereby determining how amplitude and phase change across \mathbf{k} and ω .

Time-periodic systems. If the operator $A_{\mathbf{k}}$ in Equation 1 has time-periodic coefficients, i.e., $A_{\mathbf{k}}(t) = A_{\mathbf{k}}(t + 2\pi/\omega_t)$, the steady-state response to a harmonic input with frequency ω contains an infinite number of harmonics separated by integer multiples of ω_t , i.e., $\omega + n\omega_t$, $n \in \mathbb{Z}$. The proper normal modes for frequency response analysis are no longer purely harmonic, $e^{i\omega t}$. Rather, they are determined by the *Bloch waves* (Odeh & Keller 1964), i.e., by a product of $e^{i\theta t}$ and the $2\pi/\omega_t$ periodic function in t ,

$$\mathbf{d}_{\mathbf{k}}(t) = \sum_{n=-\infty}^{\infty} \hat{\mathbf{d}}_{\mathbf{k},n}(i\theta) e^{i(\theta + n\omega_t)t}, \quad \theta \in [0, \omega_t), \quad \text{BW.}$$

where θ is the angular frequency and $\theta = 0$ and $\theta = \omega_t/2$ identify the fundamental and subharmonic modes, respectively. The steady-state response of a stable linear time-periodic system to a Bloch wave input BW is also a Bloch wave, $\boldsymbol{\xi}_{\mathbf{k}}(t) = \sum_n \hat{\boldsymbol{\xi}}_{\mathbf{k},n}(i\theta) e^{i(\theta + n\omega_t)t}$, and, for any (\mathbf{k}, θ) , the frequency response operator $T_{\mathbf{k}}(i\theta)$ maps $\hat{\mathbf{d}}_{\mathbf{k}}(i\theta) := \text{col}\{\hat{\mathbf{d}}_{\mathbf{k},n}(i\theta)\}_{n \in \mathbb{Z}}$ to $\hat{\boldsymbol{\xi}}_{\mathbf{k}}(i\theta) := \text{col}\{\hat{\boldsymbol{\xi}}_{\mathbf{k},n}(i\theta)\}_{n \in \mathbb{Z}}$, i.e., $\hat{\boldsymbol{\xi}}_{\mathbf{k}}(i\theta) = T_{\mathbf{k}}(i\theta)\hat{\mathbf{d}}_{\mathbf{k}}(i\theta)$. If the operators $B_{\mathbf{k}}$ and $C_{\mathbf{k}}$ in Equation 1 are time-invariant, for a system with $A_{\mathbf{k}}(t) = \sum_m A_{\mathbf{k},m} e^{im\omega_t t}$ we have

$$T_{\mathbf{k}}(i\theta) = C_{\mathbf{k}}(\mathcal{E}(i\theta) - A_{\mathbf{k}})^{-1} B_{\mathbf{k}}, \quad \text{FR1.}$$

where $\mathcal{E}(i\theta) := \text{diag}\{i(\theta + n\omega_t)I\}_{n \in \mathbb{Z}}$, $B_{\mathbf{k}}$ and $C_{\mathbf{k}}$ are the block-diagonal operators with $B_{\mathbf{k}}$ and $C_{\mathbf{k}}$ on the main diagonal, and $A_{\mathbf{k}} := \text{toep}\{\dots, A_{\mathbf{k},1}, A_{\mathbf{k},0}, A_{\mathbf{k},-1}, \dots\}$ is the block-Toeplitz operator (Jovanović 2008).

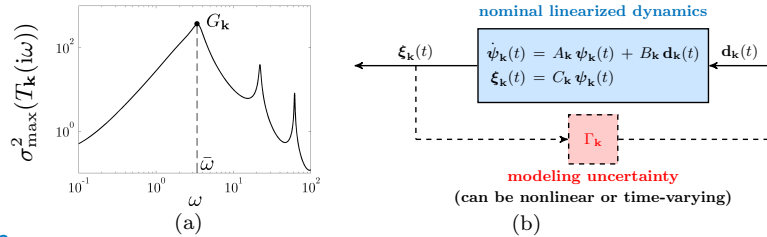


Figure 3

(a) The H_{∞} norm is determined by the peak value of $\sigma_{\max}(T_{\mathbf{k}}(i\omega))$ over ω . (b) A large H_{∞} norm of the linearized dynamics signals low robustness margins: modeling imperfections, captured by the operator $\Gamma_{\mathbf{k}}$, with the H_{∞} norm $1/\sqrt{G_{\mathbf{k}}}$ can trigger instability of $A_{\mathbf{k}} + B_{\mathbf{k}}\Gamma_{\mathbf{k}}C_{\mathbf{k}}$. This interpretation is related to the pseudo-spectra of linear operators (Trefethen & Embree 2005).

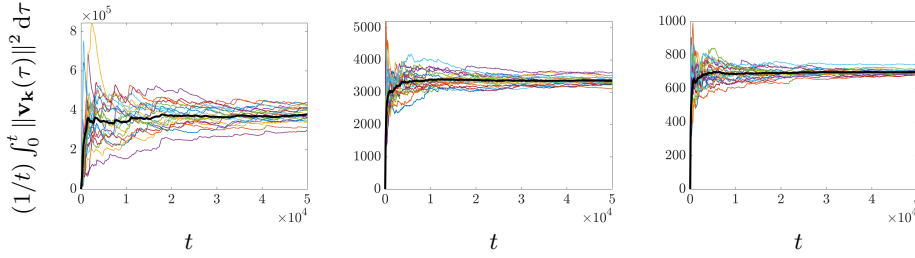


Figure 4

The variance of velocity fluctuations, $(1/t) \int_0^t \|\mathbf{v}_{\mathbf{k}}(\tau)\|_2^2 d\tau$, for 20 realizations of stochastic forcing to the linearized NS equations in Poiseuille flow with $Re = 2000$, $\mathbf{k} = (0, 1.78)$; $(1, 1)$; and $(1, 0)$. The variance averaged over all simulations is shown by a thick black line.

The Reynolds-Orr equation. In channel flow with stochastic forcing, the kinetic energy $E_{\mathbf{k}}(t) := \mathbf{E}(\langle \mathbf{v}_{\mathbf{k}}(t), \mathbf{v}_{\mathbf{k}}(t) \rangle)$ of fluctuations $\mathbf{v}_{\mathbf{k}}(t)$ around $(U(y), 0, 0)$ obeys,

$$\frac{1}{2} \frac{dE_{\mathbf{k}}(t)}{dt} = \mathbf{E} \left(\frac{1}{Re} \langle \mathbf{v}_{\mathbf{k}}(t), \Delta \mathbf{v}_{\mathbf{k}}(t) \rangle - \langle u_{\mathbf{k}}(t), U' v_{\mathbf{k}}(t) \rangle + \langle \mathbf{v}_{\mathbf{k}}(t), \mathbf{d}_{\mathbf{k}}(t) \rangle \right).$$

Here, \mathbf{E} is the expectation operator, $\langle \cdot, \cdot \rangle$ is the $L_2[-1, 1]$ inner product, $U'(y) := dU(y)/dy$, and the terms on the right-hand side denote the viscous energy dissipation, the energy exchange with the base shear, and the work done by the body forces, respectively. The nonlinear terms in the NS equations are conservative and the Reynolds-Orr equation takes the same form for nonlinear and linearized dynamics (Schmid & Henningson 2001). Since it is driven by the terms that need to be determined by solving the equations for flow fluctuations, it is not in the form which allows for direct determination of its solution. For the linearized NS equations, both the kinetic energy and the terms on the right-hand side of the Reynolds-Orr equation can be computed using the solution to differential Lyapunov equation DL, that we present below. This avoids the need for costly stochastic simulations and provides an alternative way for solving an important equation in fluid mechanics.

Time-invariant systems. Let System 1, with the output $\boldsymbol{\xi}_{\mathbf{k}}(t) = \mathbf{v}_{\mathbf{k}}(t)$, be driven by a stochastic input $\mathbf{d}_{\mathbf{k}}(t)$ with the spectral density $\Omega_{\mathbf{k}}(i\omega)$. The spectral density operator $S_{\mathbf{k}}(i\omega) = T_{\mathbf{k}}(i\omega)\Omega_{\mathbf{k}}(i\omega)T_{\mathbf{k}}^{\dagger}(i\omega)$ quantifies the two-point correlations of $\mathbf{v}_{\mathbf{k}}(t)$ across the wavenumber \mathbf{k} and the frequency ω , where $T_{\mathbf{k}}(i\omega)$ is the frequency response given in Equation FR. The inverse Fourier transform of $S_{\mathbf{k}}(i\omega)$ yields the lagged covariance operator,

$$P_{\mathbf{k}}(\tau) := \lim_{t \rightarrow \infty} \mathbf{E}(\mathbf{v}_{\mathbf{k}}(t) \otimes \mathbf{v}_{\mathbf{k}}(t + \tau)) = \frac{1}{2\pi} \int_{-\infty}^{+\infty} S_{\mathbf{k}}(i\omega) e^{i\omega\tau} d\omega,$$

where \otimes denotes the tensor product. Furthermore, the integration of $S_{\mathbf{k}}(i\omega)$ over ω yields the steady-state two-point correlation (i.e., covariance) operator $V_{\mathbf{k}}$ of the output $\mathbf{v}_{\mathbf{k}}(t)$,

$$V_{\mathbf{k}} := P_{\mathbf{k}}(0) = \lim_{t \rightarrow \infty} V_{\mathbf{k}}(t) = \frac{1}{2\pi} \int_{-\infty}^{+\infty} S_{\mathbf{k}}(i\omega) d\omega,$$

where $V_{\mathbf{k}}(t) := \mathbf{E}(\mathbf{v}_{\mathbf{k}}(t) \otimes \mathbf{v}_{\mathbf{k}}(t))$ is the time-dependent covariance operator of velocity fluctuations. For System 1, $V_{\mathbf{k}}(t) = C_{\mathbf{k}} X_{\mathbf{k}}(t) C_{\mathbf{k}}^{\dagger}$, where $X_{\mathbf{k}}(t) := \mathbf{E}(\boldsymbol{\psi}_{\mathbf{k}}(t) \otimes \boldsymbol{\psi}_{\mathbf{k}}(t))$ is the covariance operator of the state $\boldsymbol{\psi}_{\mathbf{k}}(t)$ and $C_{\mathbf{k}}^{\dagger}$ is the adjoint of the operator $C_{\mathbf{k}}$. In channel flow, for any \mathbf{k} , $V_{\mathbf{k}}$ is an operator in the wall-normal direction, $\mathbf{g}_{\mathbf{k}}(y_1) := [V_{\mathbf{k}} \mathbf{f}_{\mathbf{k}}(\cdot)](y_1)$,

whose kernel representation determines all stationary two-point correlations of $\mathbf{v}_{\mathbf{k}}(t)$,

$$\mathbf{g}_{\mathbf{k}}(y_1) = \int_{-1}^1 V_{\mathbf{k}}^{\text{ker}}(y_1, y_2) \mathbf{f}_{\mathbf{k}}(y_2) dy_2 = \int_{-1}^1 \lim_{t \rightarrow \infty} \mathbf{E}(\mathbf{v}_{\mathbf{k}}(y_1, t) \mathbf{v}_{\mathbf{k}}^*(y_2, t)) \mathbf{f}_{\mathbf{k}}(y_2) dy_2.$$

One- and two-point correlations in y are obtained for $y_1 = y_2$ and $y_1 \neq y_2$, respectively; $V_{\mathbf{k}}^{\text{ker}}(y_1, y_2)$ determines the two-point spectral density tensor and its inverse Fourier transform gives the two-point correlation tensor in x and z (Moin & Moser 1989).

Lyapunov equation. For a zero-mean temporally uncorrelated input $\mathbf{d}_{\mathbf{k}}(t)$ with the covariance operator $W_{\mathbf{k}}$, i.e., $\mathbf{E}(\mathbf{d}_{\mathbf{k}}(t)) = 0$, $\mathbf{E}(\mathbf{d}_{\mathbf{k}}(t) \otimes \mathbf{d}_{\mathbf{k}}(\tau)) = W_{\mathbf{k}} \delta(t - \tau)$, the input spectral density $\Omega_{\mathbf{k}}(i\omega)$ is constant across ω , i.e., $\Omega_{\mathbf{k}}(i\omega) = W_{\mathbf{k}}$. In this case, as described in the sidebar LYAPUNOV EQUATION: TWO-POINT CORRELATIONS, the covariance operator $X_{\mathbf{k}}(t)$ of the state $\psi_{\mathbf{k}}(t)$ in System 1 satisfies the differential Lyapunov equation,

$$\frac{dX_{\mathbf{k}}(t)}{dt} = A_{\mathbf{k}} X_{\mathbf{k}}(t) + X_{\mathbf{k}}(t) A_{\mathbf{k}}^{\dagger} + B_{\mathbf{k}} W_{\mathbf{k}} B_{\mathbf{k}}^{\dagger}. \quad \text{DL.}$$

For System 1 with the input covariance $W_{\mathbf{k}}$ and the initial condition $X_{\mathbf{k}}(0)$, this *operator-valued differential equation* can be used to compute $X_{\mathbf{k}}(t)$ and determine energy of fluctuations via $E_{\mathbf{k}}(t) = \text{trace}(C_{\mathbf{k}} X_{\mathbf{k}}(t) C_{\mathbf{k}}^{\dagger})$. For linearly unstable flows, the steady-state limit of $X_{\mathbf{k}}(t)$ is either unbounded or it does not exist. However, the solution of Equation DL can still be computed, e.g., by forward marching in time or via the following formula,

$$X_{\mathbf{k}}(t) = e^{A_{\mathbf{k}} t} X_{\mathbf{k}}(0) e^{A_{\mathbf{k}}^{\dagger} t} + \left[\begin{array}{c} I \\ 0 \end{array} \right] \exp \left(\left[\begin{array}{cc} A_{\mathbf{k}} & B_{\mathbf{k}} W_{\mathbf{k}} B_{\mathbf{k}}^{\dagger} \\ 0 & -A_{\mathbf{k}}^{\dagger} \end{array} \right] t \right) \left[\begin{array}{c} 0 \\ I \end{array} \right] e^{A_{\mathbf{k}}^{\dagger} t}.$$

In the absence of modal instability, $X_{\mathbf{k}} := \lim_{t \rightarrow \infty} X_{\mathbf{k}}(t)$ is well-defined and the steady-state limit of Equation DL is given by,

$$A_{\mathbf{k}} X_{\mathbf{k}} + X_{\mathbf{k}} A_{\mathbf{k}}^{\dagger} = -B_{\mathbf{k}} W_{\mathbf{k}} B_{\mathbf{k}}^{\dagger}. \quad \text{AL.}$$

In this case, $X_{\mathbf{k}}(t)$ can be computed from the solution $X_{\mathbf{k}}$ to the algebraic Lyapunov equation AL and the initial condition $X_{\mathbf{k}}(0)$ via $X_{\mathbf{k}}(t) = X_{\mathbf{k}} - e^{A_{\mathbf{k}} t} (X_{\mathbf{k}} - X_{\mathbf{k}}(0)) e^{A_{\mathbf{k}}^{\dagger} t}$, and the steady-state limit of $E_{\mathbf{k}}(t)$ determines the energy amplification $E_{\mathbf{k}} := \lim_{t \rightarrow \infty} E_{\mathbf{k}}(t) = \text{trace}(C_{\mathbf{k}} X_{\mathbf{k}} C_{\mathbf{k}}^{\dagger})$; see the sidebar POWER SPECTRAL DENSITY AND ENERGY AMPLIFICATION. Finally, for colored-in-time input $\mathbf{d}_{\mathbf{k}}(t)$, $X_{\mathbf{k}}$ satisfies,

$$A_{\mathbf{k}} X_{\mathbf{k}} + X_{\mathbf{k}} A_{\mathbf{k}}^{\dagger} = -(B_{\mathbf{k}} H_{\mathbf{k}}^{\dagger} + H_{\mathbf{k}} B_{\mathbf{k}}^{\dagger}), \quad \text{ALc.}$$

where the operator $H_{\mathbf{k}}$ determines the stationary cross-correlation between the input $\mathbf{d}_{\mathbf{k}}(t)$ and the state $\psi_{\mathbf{k}}(t)$ in Equation 1 (Zare et al. 2017b, Appendix B).

Departure from the white-in-time restriction removes sign-definiteness requirement on the right-hand-side in Equation AL: while the operator $B_{\mathbf{k}} W_{\mathbf{k}} B_{\mathbf{k}}^{\dagger}$ in Equation AL has non-negative eigenvalues, $B_{\mathbf{k}} H_{\mathbf{k}}^{\dagger} + H_{\mathbf{k}} B_{\mathbf{k}}^{\dagger}$ in Equation ALc is allowed to be sign-indefinite which provides additional flexibility. Furthermore, for a zero-mean white input $\mathbf{w}_{\mathbf{k}}(t)$ with the covariance operator $W_{\mathbf{k}}$, the stationary covariance operator of $\psi_{\mathbf{k}}(t)$ in the system

$$\frac{d}{dt} \begin{bmatrix} \psi_{\mathbf{k}}(t) \\ \phi_{\mathbf{k}}(t) \end{bmatrix} = \begin{bmatrix} A_{\mathbf{k}} & -B_{\mathbf{k}} K_{\mathbf{k}} \\ 0 & A_{\mathbf{k}} - B_{\mathbf{k}} K_{\mathbf{k}} \end{bmatrix} \begin{bmatrix} \psi_{\mathbf{k}}(t) \\ \phi_{\mathbf{k}}(t) \end{bmatrix} + \begin{bmatrix} B_{\mathbf{k}} \\ B_{\mathbf{k}} \end{bmatrix} \mathbf{w}_{\mathbf{k}}(t), \quad 10.$$

LYAPUNOV EQUATION: TWO-POINT CORRELATIONS OF LINEAR SYSTEMS

The Lyapunov equation can be used to propagate two-point correlations of the white stochastic input $\mathbf{d}(t)$ into colored statistics of the state $\boldsymbol{\psi}(t)$ of a linear systems (Bamieh & Dahleh 2001, Appendix A). Herein, we derive the Lyapunov equation for a finite-dimensional discrete-time LTI system,

$$\boldsymbol{\psi}(t+1) = A\boldsymbol{\psi}(t) + B\mathbf{d}(t), \quad \text{DT.}$$

where time t is a non-negative integer and A, B are constant matrices. The derivation for continuous-time systems is standard (Kwakernaak & Sivan 1972, Chapter 1.11) but is more involved and less intuitive. Let $X(t) := \mathbf{E}(\boldsymbol{\psi}(t)\boldsymbol{\psi}^*(t))$ be the covariance matrix of the state at time t , where \mathbf{E} is the expectation operator and $\boldsymbol{\psi}^*(t)$ is the complex-conjugate transpose of the vector $\boldsymbol{\psi}(t)$. Then, Equation DT can be used to write,

$$\begin{aligned} X(t+1) &= \mathbf{E}((A\boldsymbol{\psi}(t) + B\mathbf{d}(t))(\boldsymbol{\psi}^*(t)A^* + \mathbf{d}^*(t)B^*)) \\ &= A\mathbf{E}(\boldsymbol{\psi}(t)\boldsymbol{\psi}^*(t))A^* + B\mathbf{E}(\mathbf{d}(t)\boldsymbol{\psi}^*(t))A^* + A\mathbf{E}(\boldsymbol{\psi}(t)\mathbf{d}^*(t))B^* + B\mathbf{E}(\mathbf{d}(t)\mathbf{d}^*(t))B^*. \end{aligned} \quad 5.$$

If the stochastic input is white-in-time with the covariance matrix W , i.e., $\mathbf{E}(\mathbf{d}(t)\mathbf{d}^*(\tau)) = W\delta(t-\tau)$, where δ is the Kronecker delta, the cross terms in Equation 5 disappear and we obtain the Lyapunov equation,

$$X(t+1) = AX(t)A^* + BWB^*, \quad X(0) = X_0. \quad 6.$$

If the matrices A and B in Equation DT as well as the matrices W and X_0 are known, this deterministic equation can be propagated forward in time to obtain the covariance matrix $X(t)$. Even though the above derivation holds irrespective of stability properties of System DT, the steady-state limit, $X := \lim_{t \rightarrow \infty} X(t)$, only exists for stable systems. In this case, Equation 6 converges to the algebraic Lyapunov equation,

$$AXA^* - X = -BWB^*, \quad 7.$$

which is linear in X and it is typically used to compute the stationary covariance matrix X for given A, B , and W . For colored in-time stochastic inputs $\mathbf{d}(t)$, the cross terms in Equation 5 are non-zero and introducing the matrix $H(t) := A\mathbf{E}(\boldsymbol{\psi}(t)\mathbf{d}^*(t)) + \frac{1}{2}B\mathbf{E}(\mathbf{d}(t)\mathbf{d}^*(t))$ in Equation 5 allows us to write it as,

$$X(t+1) = AX(t)A^* + BH^*(t) + H(t)B^*, \quad X(0) = X_0. \quad 8.$$

For stable System DT, Equation 8 converges asymptotically to the algebraic Lyapunov-like equation,

$$AXA^* - X = -(BH^* + HB^*), \quad 9.$$

where $H := \lim_{t \rightarrow \infty} H(t)$. For continuous-time systems, Equation 6 takes the form of the differential Lyapunov equation DL which, for stable systems, converges to the algebraic Lyapunov equation AL. While Equations 5, 6, and 8 also hold for systems in which the matrices $A(t)$ and $B(t)$ depend on time, their steady-state limits may not be well-defined. Finally, for infinite-dimensional systems, the complex-conjugate transpose of a matrix, e.g., A^* , should be replaced with an adjoint of an operator, e.g., A^\dagger .

with $K_{\mathbf{k}} := ((1/2)W_{\mathbf{k}}B_{\mathbf{k}}^\dagger - H_{\mathbf{k}}^\dagger)X_{\mathbf{k}}^{-1}$, is given by $X_{\mathbf{k}}$ (Zare et al. 2017b). The $\boldsymbol{\phi}_{\mathbf{k}}$ -subsystem in Equation 10 maps the white input $\mathbf{w}_{\mathbf{k}}(t)$ to the colored input $\mathbf{d}_{\mathbf{k}}(t)$ in System 1 such that $X_{\mathbf{k}} = \lim_{t \rightarrow \infty} \mathbf{E}(\boldsymbol{\psi}_{\mathbf{k}}(t) \otimes \boldsymbol{\psi}_{\mathbf{k}}(t))$. Equivalently, the mapping from $\mathbf{w}_{\mathbf{k}}(t)$ to $\boldsymbol{\psi}_{\mathbf{k}}(t)$ in

Equation 10 can be represented via,

$$\frac{d\psi_{\mathbf{k}}(t)}{dt} = (A_{\mathbf{k}} - B_{\mathbf{k}}K_{\mathbf{k}})\psi_{\mathbf{k}}(t) + B_{\mathbf{k}}\mathbf{w}_{\mathbf{k}}(t), \quad 11.$$

and the algebraic Lyapunov Equation AL can be used to verify that the stationary two-point correlation operator of $\psi_{\mathbf{k}}(t)$ is indeed given by $X_{\mathbf{k}}$. Thus, the *impact of a colored-in-time input can be interpreted as a state-feedback modification* of the operator $A_{\mathbf{k}}$ in Equation 1.

For a stable stochastically-forced System 1, algebraic Relation ALc identifies admissible steady-state covariance operators. This fundamental relation was recently utilized for low-complexity stochastic dynamical modeling of turbulent flows (Zare et al. 2017b,a, 2020).

Time-periodic systems. The response of a linear time-periodic System 1 to a stationary stochastic input is a cyclo-stationary process (Gardner 1990); the covariance operator of the state is $2\pi/\omega_t$ periodic, i.e., $X_{\mathbf{k}}(t) := \mathbf{E}(\psi_{\mathbf{k}}(t) \otimes \psi_{\mathbf{k}}(t)) = \sum_n X_{\mathbf{k},n} e^{in\omega_t t}$, with $X_{\mathbf{k},-n} = X_{\mathbf{k},n}^\dagger$, and the effect of the stationary input, over one period $T := 2\pi/\omega_t$, is determined by $(1/T) \int_0^T X_{\mathbf{k}}(t) dt = X_{\mathbf{k},0}$. If the stochastic input $\mathbf{d}_{\mathbf{k}}(t)$ is white-in-time with the spatial covariance $W_{\mathbf{k}}$, the harmonic Lyapunov equation,

$$(A_{\mathbf{k}} - \mathcal{E}(i0))\mathcal{X}_{\mathbf{k}} + \mathcal{X}_{\mathbf{k}}(A_{\mathbf{k}} - \mathcal{E}(i0))^\dagger = -B_{\mathbf{k}}W_{\mathbf{k}}B_{\mathbf{k}}^\dagger, \quad \text{HLE.}$$

can be used to compute the Fourier series coefficients $X_{\mathbf{k},n}$ of $X_{\mathbf{k}}(t)$. Here, $A_{\mathbf{k}}$, $B_{\mathbf{k}}$, and \mathcal{E} are defined in the sidebar FREQUENCY RESPONSE OPERATOR, $W_{\mathbf{k}}$ is the block-diagonal operator with $W_{\mathbf{k}}$ on the main diagonal, and $\mathcal{X}_{\mathbf{k}}$ is the self-adjoint block-Toeplitz operator whose elements are determined by $X_{\mathbf{k},n}$ (Jovanović 2008, Jovanović & Fardad 2008).

3. UNCOVERING MECHANISMS IN WALL-BOUNDED SHEAR FLOWS

We next illustrate how the input-output approach provides insights into the physics of transitional and turbulent wall-bounded shear flows of Newtonian and viscoelastic fluids. In addition to offering a computational framework that quantifies impact of modeling imperfections on relevant flow quantities, a control-theoretic viewpoint also reveals influence of dimensionless groups on amplification of deterministic as well as stochastic disturbances and uncovers mechanisms that may initiate bypass transition. In Section 3.1, we highlight how streamwise streaks, oblique waves, and Orr-Sommerfeld modes are identified as input-output resonances of the operator that maps forcing fluctuations to different velocity components in Newtonian fluids. In Section 3.2, we demonstrate how a control-theoretic approach discovers a viscoelastic analogue of the familiar inertial lift-up mechanism, thereby identifying mechanisms that may trigger transition to elastic turbulence in rectilinear flows of viscoelastic fluids. Finally, in Section 3.3, we offer a brief overview of the merits and the effectiveness of the input-output analysis in turbulent channel and pipe flows of Newtonian fluids.

3.1. Bypass transition in channel flows of Newtonian fluids

For Poiseuille flow with $Re = 2000$, **Figure 4** shows that the streamwise constant flow structures with $k_z = 1.78$ are much more energetic than the oblique waves ($k_x = k_z = 1$) and the Orr-Sommerfeld modes ($k_x = 1, k_z = 0$). We next illustrate how the tools of Section 2.3 offer insights into the physics of transitional flows while avoiding need for stochastic simulations. **Figure 5** displays the joint impact of forcing fluctuations in all three spatial directions on the individual velocity components. For a channel-wide forcing $\mathbf{d}_{\mathbf{k}}(t)$,

Dimensionless NS equations: in incompressible Newtonian fluids with density ρ , we scale length with the channel half-height h , velocity with \bar{u} , time with the inertial time scale h/\bar{u} , pressure with $\rho\bar{u}^2$, and forcing per unit mass with \bar{u}^2/h . In analysis of transition, \bar{u} is the largest velocity of the laminar base flow and, in analysis of turbulence, \bar{u} is the friction velocity.

POWER SPECTRAL DENSITY AND ENERGY AMPLIFICATION

The power spectral density quantifies the energy of the output $\boldsymbol{\xi}_{\mathbf{k}}(t)$ of stochastically-forced System 1 across the wavenumber \mathbf{k} and temporal frequency ω ,

$$\Pi_{\mathbf{k}}(\omega) := \text{trace}(S_{\mathbf{k}}(i\omega)) = \text{trace}\left(T_{\mathbf{k}}(i\omega)\Omega_{\mathbf{k}}(i\omega)T_{\mathbf{k}}^{\dagger}(i\omega)\right),$$

where $T_{\mathbf{k}}(i\omega)$ is the frequency response and $\Omega_{\mathbf{k}}(i\omega)$ is the spectral density of $\mathbf{d}_{\mathbf{k}}(t)$. At any \mathbf{k} , the temporal-average of $\Pi_{\mathbf{k}}(\omega)$ determines the energy (variance) amplification of harmonic (in homogeneous spatial directions) stochastic (in inhomogeneous directions and time) disturbances to the linearized NS equations,

$$E_{\mathbf{k}} := \frac{1}{2\pi} \int_{-\infty}^{\infty} \Pi_{\mathbf{k}}(\omega) d\omega.$$

This quantity is also known as the *ensemble-average energy density* of the statistical steady-state, and it is hereafter referred to as the (steady-state) *energy amplification* (or energy density). For white-in-time inputs $\mathbf{d}_{\mathbf{k}}(t)$ with $\Omega_{\mathbf{k}}(i\omega) = W_{\mathbf{k}}$, the solution to the algebraic Lyapunov equation AL can be used to compute $E_{\mathbf{k}}$,

$$E_{\mathbf{k}} = \text{trace}\left(C_{\mathbf{k}}X_{\mathbf{k}}C_{\mathbf{k}}^{\dagger}\right), \tag{EA}$$

thereby avoiding integration over ω . When the input is uncorrelated in inhomogeneous spatial directions with $W_{\mathbf{k}} = I$, the sum of squares of the singular values of $T_{\mathbf{k}}(i\omega)$ gives the power spectral density, i.e., the Hilbert-Schmidt norm of $T_{\mathbf{k}}(i\omega)$. In this case, $E_{\mathbf{k}}$ determines the H_2 norm of System 1 and Parseval's identity yields,

$$E_{\mathbf{k}} = \frac{1}{2\pi} \int_{-\infty}^{\infty} \sum_{j=1}^{\infty} \sigma_{\mathbf{k},j}^2(\omega) d\omega = \frac{1}{2\pi} \int_{-\infty}^{\infty} \text{trace}\left(T_{\mathbf{k}}(i\omega)T_{\mathbf{k}}^{\dagger}(i\omega)\right) d\omega = \int_{-\infty}^{\infty} \text{trace}\left(T_{\mathbf{k}}(t)T_{\mathbf{k}}^{\dagger}(t)\right) dt.$$

Thus, in addition to quantifying the steady-state variance of System 1 subject to spatially and temporally uncorrelated stochastic inputs, the H_2 norm also determines the L_2 -norm of the impulse response and the same control-theoretic quantity enjoys both stochastic and deterministic interpretations.

Comparison of H_2 and H_{∞} norms. For flows without homogeneous directions, these two quantities compress the dynamics into a single positive number; otherwise, they are parameterized by the wavenumber \mathbf{k} . Section 2.2 offers interpretations of the H_{∞} norm and this sidebar discusses the H_2 norm. Herein, we highlight how these measures of input-output amplification of System 1 compress information in inhomogeneous directions and in time; while the H_{∞} norm maximizes over both spatial profiles and frequency by computing the temporal supremum of $\sigma_{\max}(T_{\mathbf{k}}(i\omega))$, the H_2 norm quantifies the aggregate effect of inputs by integrating the sum of squares of the singular values of $T_{\mathbf{k}}(i\omega)$ over ω .

we utilize Equation EA to evaluate the impact of the wavenumbers k_x and k_z on the steady-state variance of u , v , and w . The streamwise velocity component u contains most energy and the strongest amplification occurs in the dark red region that corresponds to small values of k_x and $O(1)$ values of k_z . The oblique modes (i.e., the flow structures with $O(1)$ values of k_x and k_z) emerge as input-output resonances in the response of the spanwise velocity w and they are significantly less amplified than the streamwise elongated flow structures with $k_x \approx 0$. On the other hand, the least-stable Orr-Sommerfeld mode, which is the dominant source of amplification for the wall-normal velocity v , creates only a local peak around ($k_x \approx 1, k_z =$

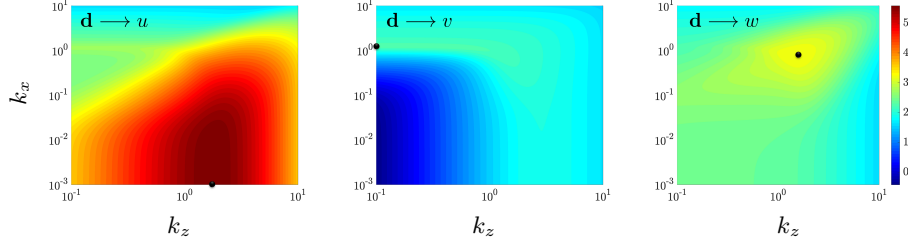


Figure 5

Energy amplification of streamwise (left), wall-normal (middle), and spanwise (right) velocity fluctuations for the linearized NS equations subject to channel-wide stochastic forcing in Poiseuille flow with $Re = 2000$. The largest value in each plot is marked by a black dot and a logarithmic scaling with the same color map is employed. The streamwise velocity contains most energy and the dominant flow structures are given by the streamwise elongated spanwise periodic streaks.

0) in the response of u . Thus, the flow structures that are deemed important in classical hydrodynamic stability play a marginal role in amplification of stochastic disturbances. This identifies shortcomings of modal stability theory, highlights the utility of componentwise input-output analysis (Jovanović & Bamieh 2005), and demonstrates that significant insight can be gained by examining linearized dynamics in the presence of modeling imperfections (in this case, additive stochastic disturbances).

3.1.1. Streamwise constant model: lift-up mechanism. In addition to computational advantages, a control-theoretic viewpoint also uncovers mechanisms for subcritical transition and quantifies impact of the Reynolds number on amplification of deterministic as well as stochastic disturbances (Jovanović 2004, Jovanović & Bamieh 2005). By considering how the disturbances propagate through the linearized dynamics, important insight can be gained *without any computations*. Since the streamwise constant fluctuations experience the largest amplification (see **Figure 5**), we examine System 1 for $\mathbf{k} := (k_x, k_z) = (0, k_z)$,

$$\begin{aligned} \frac{d}{dt} \begin{bmatrix} v(t) \\ \eta(t) \end{bmatrix} &= \overbrace{\begin{bmatrix} \frac{1}{Re} A_{os} & 0 \\ A_{cp1} & \frac{1}{Re} A_{sq} \end{bmatrix}}^{\text{non-normal}} \begin{bmatrix} v(t) \\ \eta(t) \end{bmatrix} + \begin{bmatrix} 0 & B_2 & B_3 \\ B_1 & 0 & 0 \end{bmatrix} \begin{bmatrix} d_1(t) \\ d_2(t) \\ d_3(t) \end{bmatrix}, & \quad 2D3C. \\ \begin{bmatrix} u(t) \\ v(t) \\ w(t) \end{bmatrix} &= \begin{bmatrix} 0 & C_u \\ C_v & 0 \\ C_w & 0 \end{bmatrix} \begin{bmatrix} v(t) \\ \eta(t) \end{bmatrix}, \end{aligned}$$

Normal operator: an operator is normal if it commutes with its adjoint. A normal operator is unitarily diagonalizable (i.e., it has a complete set of orthogonal eigenfunctions).

where we suppress the dependence on the spanwise wavenumber k_z . Here, v and η denote the wall-normal velocity and vorticity fluctuations, whereas (d_1, d_2, d_3) and (u, v, w) are the forcing and velocity fluctuations in (x, y, z) . The Orr-Sommerfeld, Squire, and Coupling operators are given by $A_{os} := \Delta^{-1} \Delta^2$, $A_{sq} := \Delta$, and $A_{cp1} := -ik_z U'(y)$, where $\Delta = \partial_{yy} - k_z^2 I$ is a Laplacian with homogeneous Dirichlet boundary conditions, Δ^{-1} is the inverse of the Laplacian, $\Delta^2 = \partial_{yyyy} - 2k_z^2 \partial_{yy} + k_z^4 I$ with homogeneous Dirichlet and Neumann boundary conditions, and $U'(y) = dU(y)/dy$. We refer the reader to Jovanović & Bamieh (2005, Section 4) for a definition of the input and output operators B and C .

As described in the sidebar BLOCK DIAGRAMS, this control-theoretic tool decomposes complex systems into essential pieces, abstract unnecessary details, and highlight the flow of information. A graphical representation of the frequency response operator in **Figure 6(a)** illustrates that the wall-normal and spanwise forcing fluctuations (d_2, d_3) produce $O(Re)$

fluctuations in v and w . Although these are dissipated by viscosity, the resulting spanwise variations in v , $ik_z v$, tilt the spanwise vorticity of the laminar base flow, $-U'(y)$, in the wall-normal direction y , thereby triggering $O(Re^2)$ fluctuations in η and, consequently, in $u = \eta/(ik_z)$. This *lift-up mechanism* (Landahl 1975) is a dominant source of amplification in wall-bounded shear flows of Newtonian fluids. The operator A_{cp1} acts as a *source in the wall-normal vorticity equation* and it accounts for *vortex tilting* which arises from *linearization of the convective terms* in the NS equations. Since A_{os} and A_{sq} are self-adjoint, in the absence of vortex tilting the dynamics are characterized by viscous dissipation.

3.2. Early stages of transition to elastic turbulence: viscoelastic lift-up

In complex fluids and complex flows, it is even more important to explicitly account for modeling imperfections by quantifying their influence on transient and asymptotic dynamics. Herein, we illustrate how input-output analysis discovers mechanisms that may initiate *by-pass transition* in channel flows of viscoelastic fluids *in the absence of inertia*. Transition in fluids that contain polymer chains can impact polymer processing and enhance micro-fluidic mixing. In contrast to Newtonian fluids, viscoelastic liquids can deviate from laminar profiles even when inertia is negligible (Groisman & Steinberg 2000) and, in curvilinear flows, a purely elastic instability triggers transition (Larson et al. 1990). In low inertial regimes, rectilinear flows are asymptotically stable but the dynamics associated with polymer stress fluctuations can still induce complex responses (Qin et al. 2019a,b). Since no single constitutive equation *fully describes the range of phenomena in viscoelastic fluids*, it is important to understand how modeling imperfections may adversely affect their dynamics.

Newtonian fluids are characterized by a static-in-time linear relation between stresses and velocity gradients. In viscoelastic fluids, constitutive equations determine the influence of velocity gradients on the dynamics of stress tensor. For dilute polymer solutions, polymer molecules are treated as springs that connect spherical beads (Bird et al. 1987); the Oldroyd-B (infinitely extensible linear spring) and the FENE-type (finitely extensible nonlinear elastic) models are most commonly used. In the absence of inertia we can set $Re = 0$ and the Weissenberg number, $We = \lambda \bar{u}/h$, and the viscosity ratio, $\beta = \mu_s/(\mu_s + \mu_p)$, characterize channel flows of Oldroyd-B fluids. The Weissenberg number quantifies the ratio between the elastic and viscous forces and it is given by the product of the polymer relaxation time λ and the velocity gradient \bar{u}/h . The steady solution determines the laminar base flow $(\bar{\mathbf{u}}, \bar{\boldsymbol{\tau}})$, where $\bar{\mathbf{u}} = (U(y), 0, 0)$, $U(y) = 1 - y^2$ in pressure-driven Poiseuille flow, $U(y) = y$ in shear-driven Couette flow, and the non-zero components of the base polymer stress tensor $\bar{\boldsymbol{\tau}}$ are $\bar{\tau}_{11} = 2We(U'(y))^2$ and $\bar{\tau}_{12} = \bar{\tau}_{21} = U'(y)$. Equations for infinitesimal velocity, pressure, and stress fluctuations are obtained by linearization around $(\bar{\mathbf{u}}, \bar{\boldsymbol{\tau}})$.

Hoda et al. (2008, 2009) were the first to investigate nonmodal amplification of disturbances in channel flows of viscoelastic fluids and demonstrate high sensitivity of the laminar flow in both inertia- and elasticity-dominated regimes. Jovanović & Kumar (2010) showed that velocity and stress fluctuations experience significant transient growth even in the absence of inertia. Jovanović & Kumar (2011) identified a new slow-fast decomposition of the governing equations and used singular-perturbation techniques to *analytically* establish unfavorable scaling of the energy amplification with the Weissenberg number in weakly-inertial flows. Lieu et al. (2013) quantified the role of finite extensibility of polymers on the worst-case amplification of disturbances in FENE-type models and Hariharan et al. (2018) studied amplification of localized body forces. The combined effects of inertia and elasticity on streak evolution was examined in Page & Zaki (2014), Agarwal et al. (2014).

Dimensionless Oldroyd-B model: in channel flows of Oldroyd-B fluids (with density ρ , solvent and polymer viscosities μ_s and μ_p), equations can be brought to a non-dimensional form by scaling length with the channel half-height h , velocity with the largest velocity of the base flow \bar{u} , time with the polymer relaxation time λ , polymer stresses with $\mu_p \bar{u}/h$, pressure with $(\mu_s + \mu_p) \bar{u}/h$, and forcing per unit mass with $(\mu_s + \mu_p) \bar{u}/\rho h^2$.

For streamwise-constant flows of Oldroyd-B fluids the block diagram in **Figure 6(b)** reflects the structure of the frequency response operator that maps disturbances to the momentum equation (inputs) to the velocity fluctuations (outputs) and eliminates all unnecessary variables. Apart from the operator $A_{cp2} := ik_z(U'(y)\Delta + 2U''(y)\partial_y)$, which accounts for *stretching of polymer stress fluctuations by a base shear*, all other operators are the same as in Newtonian fluids; see Section 3.1.1. The block diagrams reveal striking structural similarity between streamwise-constant inertial flows of Newtonian fluids and inertialess flows of viscoelastic fluids. In the absence of base shear $U'(y)$ and spanwise variations in fluctuations, the responses of viscoelastic fluids are governed by viscous dissipation and all velocity components are We -independent. However, in contrast to Newtonian fluids, spanwise variations in fluctuations and their interactions with $U'(y)$ provide a source in the vorticity equation even in the absence of inertia. In particular, the influence of d_2 and d_3 on u can be understood by analyzing the wall-normal vorticity equation (Jovanović & Kumar 2011),

$$\beta\Delta\hat{\eta}(t) = -\Delta\eta(t) - (1 - \beta) We (U'(y)\Delta + 2U''(y)\partial_y) ik_z\vartheta(t),$$

where ϑ denotes a low-pass version of the wall-normal velocity v , $\hat{\vartheta} := \hat{v}/(i\omega + 1)$. The source term arises from stretching of polymer stress fluctuations by a base shear and it introduces a lift-up of fluctuations in a similar way as vortex tilting in inertia-dominated flows of Newtonian fluids. Thus, the wall-normal and spanwise inputs give rise to an energy transfer from the base flow to fluctuations and generate streamwise velocity fluctuations that are proportional to the Weissenberg number. Responses from all other inputs to all other velocities are We -independent and they are governed by viscous dissipation. Jovanović & Kumar (2011) also demonstrated that d_2 and d_3 induce a quadratic scaling with the Weissenberg number of the streamwise component of the polymer stress tensor, τ_{11} .

Summary. Elementary control-theoretic analysis identifies key physical mechanisms and demonstrates that the wall-normal and spanwise body forces have the largest impact on the streamwise velocity fluctuation in inertia-dominated channel flows of Newtonian fluids and elasticity-dominated flows of viscoelastic fluids. These conclusions are derived *without any computations* by examining the frequency responses of streamwise constant fluctuations and showing that d_2 and d_3 induce a quadratic scaling of u with the Reynolds number (in Newtonian fluids) and a linear scaling of u with the Weissenberg number (in inertialess Oldroyd-B fluids). At $k_x = 0$, d_1 does not influence v and w and the mappings from all other forcing to all other velocity components are proportional to the Reynolds number (in Newtonian fluids) and are We -independent (in viscoelastic fluids); see Jovanović & Bamieh (2005, Section 4) and Jovanović & Kumar (2011) for additional details. In spite of these structural similarities, amplification in Newtonian and viscoelastic fluids originates from different physical mechanisms; vortex tilting and polymer stretching, respectively.

3.3. Turbulent channel and pipe flows of Newtonian fluids

Lee et al. (1990) used DNS of homogeneous turbulence to demonstrate that the linear amplification of eddies that interact with large mean shear induces streamwise streaks even in the absence of a solid boundary. This study also employed linear rapid distortion theory (Pope 2000) to predict the lack of isotropy and the structure of turbulence at high shear rate. Furthermore, Kim & Lim (2000) used DNS of a turbulent channel flow to show decay of near-wall turbulence in the absence of the linear vortex tilting term.

In contrast to the laminar base flow, the time-averaged turbulent mean velocity is not

BLOCK DIAGRAMS: A TOOL FOR REVEALING STRUCTURE W/O COMPUTATIONS

Block diagrams decompose complex systems into essential pieces, abstract unnecessary details, and highlight the flow of information. This control-theoretic tool reveals structure without any computations and allows to make useful analogies. The circles denote summation of input signals and the boxes represent different parts of the system. Inputs into each box/circle are represented by lines with arrows directed toward the box/circle, and outputs are represented by lines with arrows leading away from the box/circle. The inputs specify the signals affecting subsystems, and the outputs specify the signals of interest or signals affecting other parts of the system. In streamwise-constant channel flows of Newtonian and inertialess viscoelastic fluids, the block diagrams in **Figure 6** illustrate influence of disturbances (d_1, d_2, d_3) to the momentum equation on the velocity fluctuations (u, v, w). The blue boxes represent resolvent operators associated with A_{os} and A_{sq} , and the red boxes represents the coupling operators $A_{cp1} := -ik_z U'(y)$ and $A_{cp2} := ik_z(U'(y)\Delta + 2U''(y)\partial_y)$. In Newtonian fluids, $\Omega := \omega Re$ is the frequency scaled with the diffusive time scale, h^2/ν , and in viscoelastic fluids, ω is the frequency scaled with the polymer relaxation time, λ .

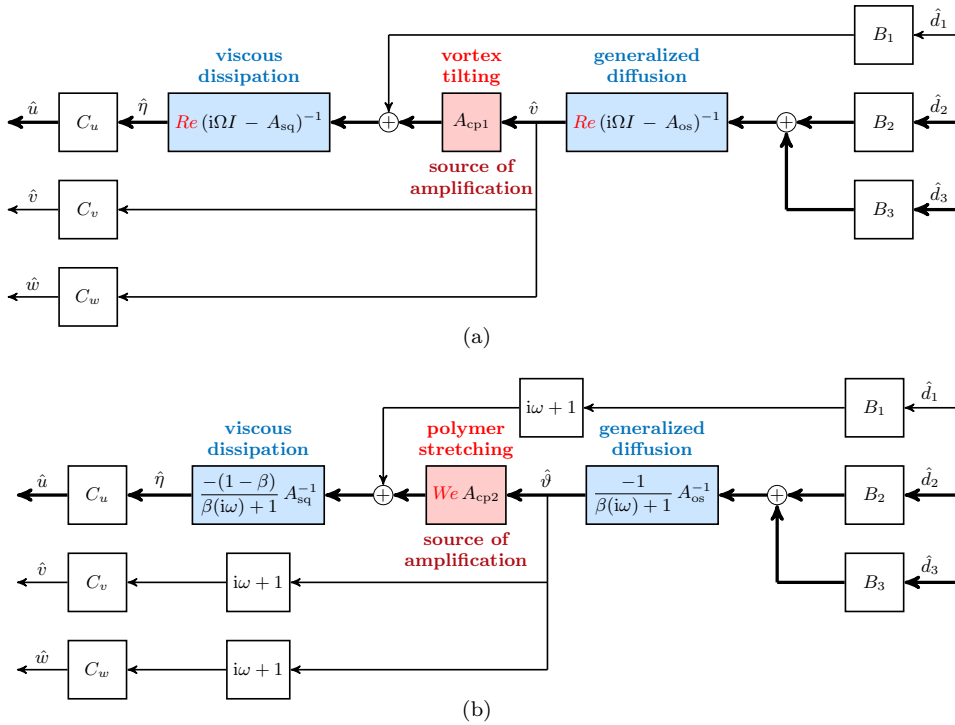


Figure 6

Block diagrams of the frequency response operators that map the forcing to the velocity fluctuations in streamwise-constant channel flows of (a) Newtonian fluids; and (b) inertialess Oldroyd-B fluids. The thick black lines indicate the part of the system responsible for large amplification. In Newtonian fluids amplification originates from vortex tilting, i.e., the operator A_{cp1} in Equation 2D3C and in viscoelastic fluids it originates from polymer stretching, i.e., the operator A_{cp2} . In Newtonian fluids, singular values of the frequency responses from d_l to r are proportional to Re^2 , for $r = u$ and $l = \{2, 3\}$; to Re , for $\{r = u, l = 1; r = \{v, w\}, l = \{2, 3\}\}$; and are equal to zero for $\{r = \{v, w\}, l = 1\}$; in inertialess flows of viscoelastic fluids, they are proportional to We , for $\{r = u, l = \{2, 3\}\}$; all other singular values are We -independent.

a solution of the NS equations and even the question of what to linearize around can be contentious (Beneddine et al. 2016). Since the linearized NS equations around the turbulent mean flow are stable (Malkus 1956, Reynolds & Tiederman 1967), they are well-suited for input-output analysis. Butler & Farrell (1993) utilized transient growth analysis over a horizon determined by the eddy turnover time to show that the streak spacing of approximately 100 wall units represents the optimal response of the NS equations linearized around the turbulent mean flow. McKeon & Sharma (2010) employed a gain-based decomposition of fluctuations around mean velocity in turbulent pipe flow to characterize energetic structures in terms of their convection speeds and wavelengths. This study highlighted the role of critical layers in wall-normal localization of experimentally identified energetic modes and related the wave speed, $c := \omega/k_x$, to the wall-normal localization of the dominant flow structures. Moarref et al. (2013) leveraged the role of wave speed to formally determine three different scalings for the most amplified modes; showed that these scales are consistent with inner, logarithmic, and outer layers in the turbulent mean velocity; and established dependence of the dominant resolvent modes on the spatial coordinates.

Other classes of linearized models have also been utilized to identify the spatio-temporal structure of the most energetic fluctuations in turbulent flows. In particular, the turbulent mean flow can be obtained as the steady-state solution of the NS equations in which molecular viscosity is augmented with turbulent eddy-viscosity (Reynolds & Tiederman 1967, Reynolds & Hussain 1972). del Álamo & Jiménez (2006), Cossu et al. (2009), Pujals et al. (2009), Hwang & Cossu (2010a,b) demonstrated that transient growth and input-output analyses of the resulting linearization qualitatively capture features of turbulent flows.

For a turbulent channel flow with $Re = 547$ and $k_x = 0$, **Figure 7** demonstrates the emergence of channel-wide and near-wall streaks in a stochastically-forced eddy-viscosity-enhanced linearized model. The values of k_z where the two peaks in the premultiplied energy spectrum $k_z E_{k_z}$ emerge determine the spanwise length scales of the most energetic response of velocity fluctuations to stochastic forcing (left plot). Streamwise velocity fluctuations that contain the most variance are harmonic in z and their wall-normal shapes are determined by the principal eigenfunctions of the stationary covariance operator V_k (middle and right plots). Pairs of counter-rotating streamwise vortices (contour lines) distribute momentum in the (y, z) -plane and promote amplification of high (hot colors) and low (cold colors) speed streamwise streaks. The most energetic flow structures occupy the entire channel width and the second set of strongly amplified fluctuations is determined by near-wall streaks.

4. CONTROL OF TRANSITIONAL AND TURBULENT FLOWS

Flow control by sensor-less means is often inspired by the desire to bring the efficiency of birds and fish to engineering systems. Control of conductive fluids using the Lorentz force, periodic blowing and suction, wall oscillations, and geometry modifications (e.g., riblets, superhydrophobic surfaces, and jet-engine chevrons) are characterized by the absence of sensing capabilities and implementation of control without measurement of the relevant flow quantities or disturbances. Rather, as illustrated in **Figure 8(a)**, the dynamics are impacted by spatio-temporal oscillations through geometry or base velocity modifications.

Min et al. (2006) used DNS to show that a blowing and suction in the form of an up-stream traveling wave can provide a *sustained sub-laminar drag* in a fully-developed turbulent channel flow. This paper inspired other researchers to examine fundamental limitations of streamwise traveling waves for control of transitional and turbulent flows (Marusic et al.

2007, Hoepffner & Fukagata 2009, Bewley 2009, Fukagata et al. 2009, Moarref & Jovanović 2010, Lieu et al. 2010). Furthermore, simulations and experiments showed that spanwise wall oscillations can reduce skin-friction drag by as much as 45% (Jung et al. 1992, Laadhari et al. 1994, Choi et al. 1998, Choi 2002, Ricco 2004). While these and other studies (e.g., Fransson et al. (2006)) demonstrate the potential of sensor-less periodic strategies, until recently a model-based design for transitional and turbulent flows remained elusive.

In Section 4.1, we highlight the utility of the input-output framework in the design of traveling waves for controlling the onset of turbulence while achieving positive net efficiency (Moarref & Jovanović 2010); and, in Section 4.2, we describe how stochastic analysis in conjunction with control-oriented turbulence modeling quantifies the effect of control on turbulent flow dynamics and identifies the optimal period of oscillations for drag reduction (Moarref & Jovanović 2012). Apart from demonstrating the merits of the input-output approach in the design of periodic strategies for controlling laminar and turbulent flows, we also illustrate how to overcome challenges that arise in “secondary receptivity analysis”, i.e., in nonmodal analysis of the dynamics associated with spatially- or time-periodic base flows.

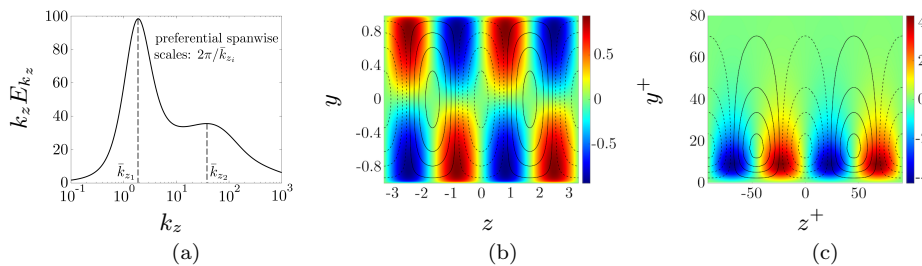


Figure 7

(a) Premultiplied energy spectrum, $k_z E_{k_z}$; and (b,c) dominant flow structures resulting from stochastically-forced eddy-viscosity enhanced linearization around the turbulent mean flow with $Re = 547$ (based on friction velocity) and $k_x = 0$. Color plots display most energetic streamwise velocity fluctuations $u(z, y)$ and contour lines show streamfunction fluctuations with the spanwise wavelength determined by (b) $2\pi/\bar{k}_{z1}$ (channel-wide streaks); and (c) $2\pi/\bar{k}_{z2}$ (near-wall streaks).

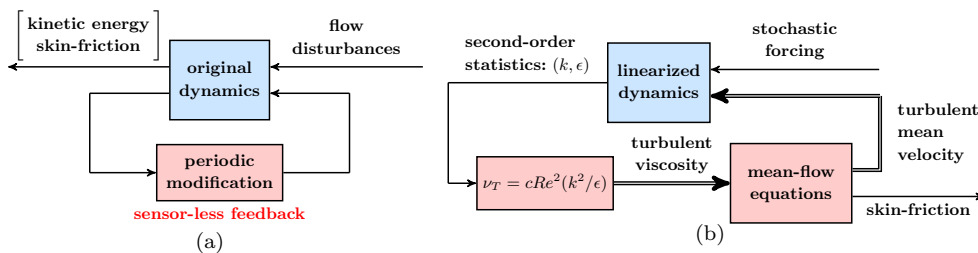


Figure 8

Block diagrams of (a) a modification to the dynamics introduced by spatio-temporal oscillations which introduce a *sensor-less feedback* by changing a base flow $U_0(y)$ to a periodic profile; and (b) a simulation-free approach for determining the influence of control on skin-friction drag in turbulent flows. The hollow arrows represent coefficients into the mean-flow and linearized equations. In Moarref & Jovanović (2012), the turbulent mean velocity is updated once.

4.1. Controlling the onset of turbulence by streamwise traveling waves

Let channel flow be subject to a uniform pressure gradient and a zero-net-mass-flux blowing and suction along the walls, $V(y = \pm 1) = \mp 2\alpha \cos(\omega_x(\bar{x} - ct))$; see **Figure 1(b)**. Here, α , ω_x , and c denote amplitude, frequency, and speed of the wave that travels in the streamwise direction \bar{x} . Positive/negative values of c identify downstream/upstream waves, and $c = 0$ gives a standing wave. The Galilean transformation, $x := \bar{x} - ct$, eliminates the time dependence in $V(\pm 1)$ and the steady-state solution of the NS equations, $\bar{\mathbf{u}} = (U(x, y), V(x, y), 0)$, does not depend on t in the frame of reference that travels with the wave. The new laminar base flow $\bar{\mathbf{u}}$ is no longer a parabola: it is periodic in x , with frequency ω_x , and it contains both streamwise and wall-normal components, $U(x, y)$ and $V(x, y)$.

4.1.1. Net efficiency of modified base flow. Blowing and suction induces a bulk flux in the direction opposite to the direction in which the wave travels (Høpfner & Fukagata 2009). This *pumping mechanism* occurs even in the absence of the pressure gradient and a weakly-nonlinear analysis explains it. For small amplitude α , $U(x, y)$ is given by

$$U(x, y) = \underbrace{U_0(y)}_{\text{parabola}} + \underbrace{\alpha^2 U_{20}(y)}_{\text{mean drift}} + \underbrace{\alpha (U_{1p}(y) e^{i\omega_x x} + U_{1m}(y) e^{-i\omega_x x}) + \alpha^2 (U_{2p}(y) e^{i2\omega_x x} + U_{2m}(y) e^{-i2\omega_x x})}_{\text{oscillatory components}} + O(\alpha^3).$$

In addition to an oscillatory $O(\alpha)$ correction to $U_0(y)$ with frequency ω_x , both the second harmonic $2\omega_x$ and the mean flow correction $U_{20}(y)$ are induced by the quadratic nonlinearity in the NS equations at the level of α^2 . For the fixed pressure gradient, the skin-friction drag coefficient of the base flow is inversely proportional to the square of the bulk flux. Since the integral of $U_{20}(y)$ is positive for the upstream and negative for the downstream waves (Høpfner & Fukagata 2009, Moarref & Jovanović 2010), upstream/downstream waves reduce/increase skin-friction drag coefficient relative to the laminar uncontrolled flow.

The net efficiency of wall-actuation is given by the difference of the produced and required powers (Quadrio & Ricco 2004). These two quantities, respectively, determine increase/decrease in bulk flux relative to the flow with no control and the control effort exerted at the walls. Compared to laminar uncontrolled flow, any strategy based on blowing and suction reduces net efficiency (Bewley 2009, Fukagata et al. 2009). However, if uncontrolled flow becomes turbulent, both upstream and downstream waves of small enough amplitudes can improve net efficiency (Moarref & Jovanović 2010, Section 2.4). Moarref & Jovanović (2010) also demonstrated that, apart from the net efficiency, *the dynamics of fluctuations around the modified base flow have to be evaluated when designing the traveling waves.*

4.1.2. Dynamics of velocity fluctuations. The laminar base flow induced by the traveling waves is periodic in x , with frequency ω_x , and the resulting linearization is not translationally-invariant in the streamwise direction. The normal modes in z are still harmonic, $e^{ik_z z}$, but in x they are given by the Bloch waves, which are determined by a product of $e^{i\theta x}$ and the $2\pi/\omega_x$ periodic function in x , $\tilde{\mathbf{d}}_{\mathbf{k}}(x, y, t) = \tilde{\mathbf{d}}_{\mathbf{k}}(x + 2\pi/\omega_x, y, t)$,

$$\mathbf{d}(x, y, z, t) = \tilde{\mathbf{d}}_{\mathbf{k}}(x, y, t) e^{i(\theta x + k_z z)} = \sum_{n=-\infty}^{\infty} \tilde{\mathbf{d}}_{\mathbf{k},n}(y, t) e^{i((\theta + n\omega_x)x + k_z z)}, \quad \theta \in [0, \omega_x),$$

where $\mathbf{k} := (\theta, k_z)$ and $\tilde{\mathbf{d}}_{\mathbf{k},n}(y, t)$ are the coefficients in the Fourier series expansions of $\tilde{\mathbf{d}}_{\mathbf{k}}(x, y, t)$. In this case, signals in Equation 1 are the \mathbf{k} -parameterized bi-infinite column vectors whose components are determined by the corresponding Fourier series coefficients,

e.g., $\mathbf{d}_{\mathbf{k}}(t) := \text{col}\{\tilde{\mathbf{d}}_{\mathbf{k},n}(y, t)\}_{n \in \mathbb{Z}}$, and similarly for $\psi_{\mathbf{k}}(t)$ and $\xi_{\mathbf{k}}(t)$. Thus, for each \mathbf{k} , $A_{\mathbf{k}}$, $B_{\mathbf{k}}$, and $C_{\mathbf{k}}$ in Equation 1 are bi-infinite matrices whose entries are operators in the wall-normal direction y (Moarref & Jovanović 2010), and the frequency response operator $T_{\mathbf{k}}(i\omega)$ in Equation FR maps $\hat{\mathbf{d}}_{\mathbf{k}}(i\omega) := \text{col}\{\tilde{\mathbf{d}}_{\mathbf{k},n}(y, i\omega)\}_{n \in \mathbb{Z}}$ to $\hat{\xi}_{\mathbf{k}}(i\omega) := \text{col}\{\tilde{\xi}_{\mathbf{k},n}(y, i\omega)\}_{n \in \mathbb{Z}}$.

Since modal stability does not capture the *early stages of transition*, Moarref & Jovanović (2010) utilized input-output analysis of a linearization around $(U(x, y), V(x, y), 0)$ to quantify the effect of control on amplification of stochastic disturbances and identify waves that reduce receptivity relative to the flow without control. A discretization in y and truncation of bi-infinite matrices in Equation 1 yield a large-scale Lyapunov Equation AL; computing its solution to assess impact of control parameters (α, ω_x, c) , wavenumbers (θ, k_z) , and the Reynolds number Re on the energy amplification is demanding. Motivated by the observation that large values of α introduce high cost of control, Moarref & Jovanović (2010) employed a perturbation analysis to efficiently compute the solution to Equation AL. This approach offers significant advantages relative to the approach based on truncation: *impact of small amplitude waves on energy amplification can be assessed via computations that are of the same complexity as computations in the uncontrolled flow*. In particular, for small amplitude waves, the following *explicit formula*,

$$\frac{\text{energy amplification with control}}{\text{energy amplification without control}} = 1 + \alpha^2 g_{\mathbf{k}}(\omega_x, c, Re) + O(\alpha^4), \quad 12.$$

offers insights into the impact of control on energy amplification. For $\alpha \ll 1$, the analysis amounts to examining the dependence of the function $g_{\mathbf{k}}$ in Equation 12 on $\mathbf{k} = (\theta, k_z)$, the frequency/speed (ω_x, c) of the wave, and the Reynolds number Re . Positive (negative) values of $g_{\mathbf{k}}$ identify parameters that increase (decrease) energy amplification. For channel flow with $Re = 2000$ and fixed values of ω_x and c , we use a sign-preserving logarithmic scale to visualize the \mathbf{k} -dependence of the function $g_{\mathbf{k}}$ in **Figure 9**. While the downstream waves with $(\omega_x = 2, c = 5)$ reduce amplification for all values of θ and k_z , the upstream waves with $(\omega_x = 0.5, c = -2)$ promote amplification for a broad range of θ and k_z . Thus, in addition to guaranteeing positive net efficiency relative to the uncontrolled flow that becomes turbulent (see Section 4.1.1), the downstream waves also suppress energy of 3D fluctuations. On the other hand, the upstream waves with the parameters that provide favorable skin-friction coefficient of the modified laminar flow (Min et al. 2006) increase amplification of the most energetic modes of the uncontrolled flow. In fact, since, at best, they exhibit receptivity similar to that of the uncontrolled flow (Moarref & Jovanović 2010) and can even induce modal instability of the modified laminar flow (Lee et al. 2008), they are not suitable for controlling the onset of turbulence. In contrast, *properly designed* downstream waves can *substantially reduce production of fluctuations' kinetic energy* (Moarref & Jovanović 2010) and they are an excellent candidate for preventing transition to turbulence.

DNS verification. All theoretical predictions resulting from a simulation-free approach of Moarref & Jovanović (2010) were verified by Lieu et al. (2010). Their DNS confirmed that the downstream waves indeed provide an effective means for controlling the onset of turbulence and that the upstream waves promote transition even when the uncontrolled flow stays laminar. This demonstrates considerable predictive power of the input-output framework and suggests that reducing receptivity is a viable approach to controlling transition.

4.2. Turbulent drag reduction by spanwise wall oscillations

Spanwise wall oscillations can reduce turbulent drag by as much as 45%. This observation was made in both simulations and experiments and theoretical studies (Dhanak & Si 1999, Bandyopadhyay 2006, Ricco & Quadrio 2008) focused on explaining the effectiveness of this sensor-less strategy. Herein, we describe how input-output analysis in conjunction with a control-oriented turbulence modeling identifies the optimal period of oscillations for turbulence suppression in channel flow; see Moarref & Jovanović (2012) for details.

Modified mean flow. In pressure-driven channel flow, the steady-state solution of the NS equations in which the molecular viscosity is augmented with the turbulent viscosity $\nu_{T0}(y)$ is determined by the Reynolds-Tiederman profile, $U_0(y)$. If the flow is also subject to $W(y = \pm 1, t) = 2\alpha \sin(\omega_t t)$, the steady-state solution is given by $(U_0(y), 0, W_0(y, t) = \alpha(W_p(y)e^{i\omega_t t} + W_p^*(y)e^{-i\omega_t t}))$. Here, $U_0(y)$ approximates the mean streamwise velocity of the uncontrolled turbulent flow and the *wall oscillations induce the time-periodic spanwise component* $W_0(y, t)$ under the assumption that the turbulent viscosity is not modified by control. If this were the case, the oscillations would have no impact on U_0 , which is at odds with simulations/experiments. In contrast, the estimates of the required power exerted by wall oscillations resulting from the use of W_0 closely match the DNS results of Quadrio & Ricco (2004) over a broad range of oscillation periods (Moarref & Jovanović 2012, Section 2.2).

Turbulence modeling. The inability of the above approach to predict drag reduction arises from the fact that the wall oscillations change the turbulent viscosity of the flow with no control. Moarref & Jovanović (2012) pioneered a method based on the stochastically-forced eddy-viscosity-enhanced NS equations linearized around $(U_0(y), 0, W_0(y, t))$ to capture the influence of control on turbulent viscosity. The approach utilizes the Boussinesq hypothesis but, in contrast to standard practice, the turbulent kinetic energy k and its rate of dissipation ϵ are computed using the second-order statistics of velocity fluctuations in the linearized model. Using analogy with homogenous isotropic turbulence, Moarref & Jovanović (2012, Section 3.1) selected spatial correlations of white-in-time forcing to provide equivalence between the 2D energy spectra of the uncontrolled turbulent flow and the flow governed by the stochastically-forced linearization around $(U_0(y), 0, 0)$. This approach was the first to utilize available DNS data (del Álamo & Jiménez 2003, del Álamo et al. 2004) of the uncontrolled turbulent flow to guide control-oriented modeling for design purposes; it takes advantage of the turbulent viscosity and the energy spectrum of the uncontrolled flow and determines the effect of control on the turbulent flow using a model-based approach.

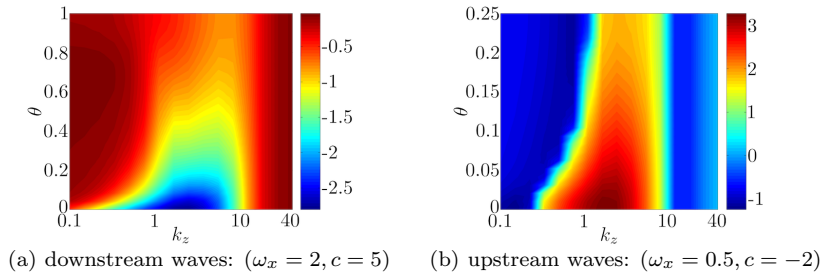


Figure 9

The second order correction to the energy amplification in Equation 12 visualized using a sign-preserving logarithmic scale, $\text{sign}(g_{\mathbf{k}}) \log_{10}(1 + |g_{\mathbf{k}}|)$, in channel flow with $Re = 2000$ (based on the centerline velocity of the parabolic laminar profile and the channel half-height). While the downstream waves with selected parameters reduce amplification for all values of θ and k_z , the upstream waves promote amplification for a broad range of θ and k_z .

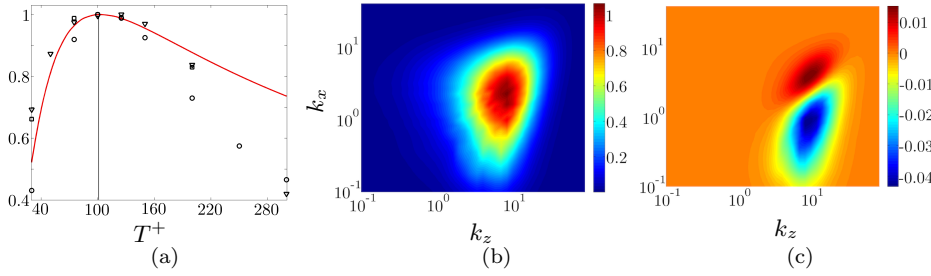


Figure 10

(a) Second-order correction (in α) to the skin-friction drag coefficient relative to the uncontrolled flow, $\%C_{f2}(T^+)$, normalized by $\max_{T^+} \%C_{f2}(T^+)$, as a function of the period of oscillations T^+ for the flow with $Re = 186$ (solid curve); DNS-based $\%C_f(T^+)$ normalized by the corresponding largest values at $Re = 200$ (Quadrio & Ricco 2004) for control amplitudes $\alpha = 2.25$, \circ ; $\alpha = 6$, \square ; and $\alpha = 9$, ∇ . (b) Premultiplied DNS-based energy spectrum, $k_x k_z E_{\mathbf{k},0}$, of the uncontrolled turbulent flow with $Re = 186$; and (c) second-order correction to the energy spectrum, $k_x k_z E_{\mathbf{k},2}$, for the flow subject to wall oscillations with optimal drag-reducing period $T^+ = 102.5$.

Dynamics of velocity fluctuations. Linearization around $(U_0(y), 0, W_0(y, t))$ yields a time-periodic model with $A_{\mathbf{k}}(t) = A_{\mathbf{k},0} + \alpha (A_{\mathbf{k},-1} e^{-i\omega t} + A_{\mathbf{k},1} e^{i\omega t})$, and the solution to Equation HLE provides two-point correlations. For small amplitude oscillations, Moarref & Jovanović (2012) utilized perturbation analysis to efficiently solve this equation and identify the oscillation periods that yield the largest drag reduction and net efficiency. This approach quantifies the influence of velocity fluctuations on the turbulent viscosity in the flow with control, $\nu_T(y) = \nu_{T0}(y) + \alpha^2 \nu_{T2}(y) + O(\alpha^4)$, where $\nu_{T0}(y)$ is the turbulent viscosity of the uncontrolled flow and $\nu_{T2}(y)$ is determined by the second-order corrections (in α) to the kinetic energy $k_2(y)$ and its rate of dissipation $\epsilon_2(y)$. These quantities are obtained by averaging the second-order statistics resulting from a stochastically-forced linearization around $(U_0(y), 0, W_0(y, t))$ over the wall-parallel directions and one period of oscillations.

The solution to Equation HLE and the above expression for ν_T are used to assess the influence of small amplitude oscillations on the dynamics of velocity fluctuations and to identify the optimal period of oscillations for drag reduction. For the controlled flow with constant bulk flux and the friction Reynolds number $Re = 186$, solid curve in **Figure 10** shows the second-order correction to the skin-friction coefficient $\%C_{f2}(T^+)$, normalized by its largest value, and symbols display normalized DNS results at $Re = 200$ (Quadrio & Ricco 2004). A close agreement between a theoretical prediction for the optimal period resulting from input-output analysis ($T^+ = 102.5$) and DNS results ($T^+ \approx 100$) is observed. Middle and right plots in **Figure 10** show the premultiplied 2D energy spectrum of the uncontrolled flow, $k_x k_z E_{\mathbf{k},0}$, and the second-order correction, $k_x k_z E_{\mathbf{k},2}$, triggered by small amplitude oscillations with the optimal period $T^+ = 102.5$. The most energetic modes of the uncontrolled flow occur at $(k_x \approx 2.5, k_z \approx 6.5)$. The red region in the right plot shows that the wall oscillations increase amplification of the modes with small streamwise wavelengths, and the blue region indicates suppression of energy of large streamwise wavelengths. This observation agrees with the study of the impact of wall oscillations on free-stream vortices in a pre-transitional boundary layer (Ricco 2011). Moarref & Jovanović (2012) also showed that the optimal wall-oscillations minimize the turbulent viscosity near the interface of the buffer and log-law layers and that oscillations are less effective at higher Reynolds numbers.

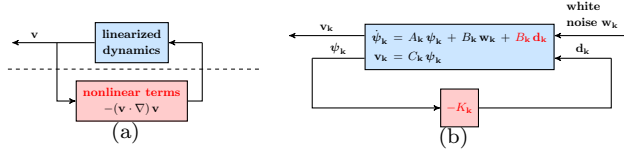


Figure 11

(a) The NS equations can be viewed as a feedback interconnection of the linearized dynamics with the nonlinear term; (b) Stochastically-driven linearized NS equations with low-rank state-feedback modification. At the level of second-order statistics, the two representations can be made equivalent by proper selection of $B_{\mathbf{k}}$ and $K_{\mathbf{k}}$; cf. Equation 11.

Summary. Traveling waves and wall oscillations introduce a *sensor-less feedback* via periodic modifications to the dynamics (see **Figure 8(a)**) by changing a base flow $U_0(y)$ to a spatially- or time-periodic profile. Depending on the actuation waveform and the parameters, the properties can be improved or made worse relative to the flow without control. In contrast to a standard approach, which employs DNS and experiments to assess sensor-less periodic strategies, Moarref & Jovanović (2010, 2012) developed a model-based framework for determining the influence of control on transitional and turbulent flows. These references demonstrate the critical importance of the dynamics associated with the modified base flows for the design of effective strategies for controlling the onset of turbulence and drag reduction. The developed simulation-free method enables computationally-efficient design by merging receptivity analysis and control-oriented turbulence modeling with techniques from control theory and its utility goes beyond the case studies presented here. Recently, input-output approach was used to quantify the effect of riblets on kinetic energy and turbulent drag in channel flow (Chavarin & Luhar 2020, Ran et al. 2020) and it is expected to enable optimal design of periodic strategies for control of transitional and turbulent flows. Input-output framework is also at the heart of the optimal and robust H_2 and H_∞ feedback control strategies (Zhou et al. 1996) and it has recently found use in the model-based design of opposition control (Luhar et al. 2014, Toedtli et al. 2019).

5. PHYSICS-AWARE DATA-DRIVEN TURBULENCE MODELING

The advances in high-performance computing and measurement techniques provide abundance of data for a broad range of flows. Thus, turbulence modeling can be formulated as an inverse problem where the objective is to identify a parsimonious model that explains available and generalizes to unavailable data. Techniques from machine learning and statistical inference were recently employed to reduce uncertainty and improve predictive power of models based on the Reynolds-Averaged NS (RANS) equations (Duraisamy et al. 2019). Large data sets can also be exploited to develop reduced dynamical representations (Rowley & Dawson 2017) but an exclusive reliance on data makes such models agnostic to physical constraints and can yield subpar performance in regimes that are not contained in the training data set. Moreover, sensing and actuation can significantly change the identified model, thereby making its use for flow control challenging (Noack et al. 2011, Tadmor & Noack 2011). A compelling alternative for model-based optimization and control is to leverage data in conjunction with a prior model that arises from first principles.

As demonstrated in Section 3, the linearized NS equations in the presence of stochastic excitation can be used to *qualitatively predict structural features* of *transitional and turbulent shear flows*. In most prior studies excitations were restricted to white-in-time stochastic processes but *this assumption is often too narrow to fully capture observed statistics of turbulent*

flows (Jovanović & Georgiou 2010). To overcome these limitations, Zare et al. (2017b,a) developed a framework to allow for colored-in-time inputs to the linearized NS equations.

We next briefly summarize how strategic use of data enhances predictive power of the linearized NS equations in order to capture second-order statistics of turbulent flows (Zare et al. 2017b,a, 2020). Since machine learning tools are physics-agnostic, the power spectrum of stochastic forcing is identified by merging tools from control theory and convex optimization. The resulting stochastic model, given by Equation 11, accounts for neglected nonlinear interactions via a low-rank perturbation to the original dynamics; see **Figure 11**.

5.1. Completion of partially available channel flow statistics

Herein, we examine linearization around mean velocity in turbulent channel flow and highlight the utility of the framework developed in Zare et al. (2017b,a). A pseudo-spectral method (Weideman & Reddy 2000) yields a finite-dimensional approximation of the operators in y and a change of variables (Zare et al. 2017b, Appendix A) leads to an evolution model in which the kinetic energy at any \mathbf{k} is determined by the Euclidean norm of the state vector $\psi_{\mathbf{k}}$. For given $(A_{\mathbf{k}}, B_{\mathbf{k}})$ and input statistics $(W_{\mathbf{k}}$ or $H_{\mathbf{k}})$, algebraic Relations AL and ALc can be used to compute the stationary covariance matrix $X_{\mathbf{k}}$ of the state $\psi_{\mathbf{k}}$ in System 1. However, in turbulence modeling, the converse question arises: starting from Model 1 and the covariance matrix $X_{\mathbf{k}}$ (resulting from DNS or experiments), can we identify the power spectrum of the stochastic input $\mathbf{d}_{\mathbf{k}}(t)$ that generates such statistics? For the NS equations linearized around turbulent mean velocity with white-in-time stochastic forcing, the answer to this question is negative (Zare et al. 2017b, Figure 6). This limitation can be overcome by allowing for colored-in-time stochastic inputs to the linearized Model 1.

The positive-definite matrix $X_{\mathbf{k}}$ is the stationary covariance of the state $\psi_{\mathbf{k}}(t)$ of linear time-invariant System 1 with controllable pair $(A_{\mathbf{k}}, B_{\mathbf{k}})$ if and only if (Georgiou 2002a,b)

$$\text{rank} \begin{bmatrix} A_{\mathbf{k}}X_{\mathbf{k}} + X_{\mathbf{k}}A_{\mathbf{k}}^* & B_{\mathbf{k}} \\ B_{\mathbf{k}}^* & 0 \end{bmatrix} = \text{rank} \begin{bmatrix} 0 & B_{\mathbf{k}} \\ B_{\mathbf{k}}^* & 0 \end{bmatrix}. \quad 13.$$

This fundamental condition guarantees that, for given $A_{\mathbf{k}}$, $B_{\mathbf{k}}$, and $X_{\mathbf{k}}$, Equation ALc can be solved for $H_{\mathbf{k}}$. It also implies that *any* $X_{\mathbf{k}} = X_{\mathbf{k}}^* > 0$ is admissible as a stationary covariance of $\psi_{\mathbf{k}}(t)$ in Equation 1 if the input matrix $B_{\mathbf{k}}$ is full rank. In particular, for $B_{\mathbf{k}} = I$, Equation ALc is satisfied with $H_{\mathbf{k}}^* = -A_{\mathbf{k}}X_{\mathbf{k}}$ and stochastically-forced System 11, which for this choice of $H_{\mathbf{k}}$ and $W_{\mathbf{k}} = I$ simplifies to $\dot{\psi}_{\mathbf{k}}(t) = -(1/2)X_{\mathbf{k}}^{-1}\psi_{\mathbf{k}}(t) + \mathbf{w}_{\mathbf{k}}(t)$, can be used to generate $X_{\mathbf{k}}$. This implies that a colored-in-time input which excites all degrees of freedom in Equation 1 can completely *cancel relevant physics* contained in $A_{\mathbf{k}}$. Thus, in data-driven turbulence modeling, it is critically important to restrict the rank of the matrix $B_{\mathbf{k}}$ which specifies the number of inputs to the linearized NS equations.

To address this challenge, Zare et al. (2017b,a) formulated and solved the problem of completing a subset of entries $V_{\mathbf{k},ij}^{\text{dns}}$ of the stationary covariance matrix $V_{\mathbf{k}}^{\text{dns}}$ of velocity fluctuations using stochastically-forced linearization around the turbulent mean velocity. The approach utilizes algebraic Relation ALc with $Z_{\mathbf{k}} := B_{\mathbf{k}}H_{\mathbf{k}}^* + H_{\mathbf{k}}B_{\mathbf{k}}^*$ and a maximum entropy formalism along with a convex surrogate for rank minimization to limit the number of inputs to the linearized model and identify spectral content of the colored-in-time forcing,

$$\begin{array}{ll} \underset{X_{\mathbf{k}}, Z_{\mathbf{k}}}{\text{minimize}} & -\log \det(X_{\mathbf{k}}) + \gamma \sum_i \sigma_i(Z_{\mathbf{k}}) & \text{objective function} \\ \text{subject to} & A_{\mathbf{k}}X_{\mathbf{k}} + X_{\mathbf{k}}A_{\mathbf{k}}^* + Z_{\mathbf{k}} = 0 & \text{physics} \\ & (C_{\mathbf{k}}X_{\mathbf{k}}C_{\mathbf{k}}^*)_{ij} = V_{\mathbf{k},ij}^{\text{dns}}, (i,j) \in \mathcal{I}. & \text{available data} \end{array} \quad \text{CC.}$$

The Hermitian matrices $X_{\mathbf{k}} \succ 0$ and $Z_{\mathbf{k}}$ are the optimization variables, whereas the matrices $(A_{\mathbf{k}}, C_{\mathbf{k}})$, the available entries $V_{\mathbf{k},ij}^{\text{dns}}$ of $V_{\mathbf{k}}^{\text{dns}}$ for a selection of indices $(i, j) \in \mathcal{I}$, and $\gamma > 0$ are known problem parameters. The first constraint in CC comes from physics and it imposes the requirement that second-order statistics are consistent with linearization around turbulent mean velocity; and the second constraint requires that the available elements of the matrix $V_{\mathbf{k}}^{\text{dns}}$ are exactly reproduced by the linearized model. The logarithmic barrier function is introduced to ensure positive-definiteness of $X_{\mathbf{k}}$ (Boyd & Vandenberghe 2004) and the sum of singular values of the matrix $Z_{\mathbf{k}}$, which reflects contribution of the stochastic input, is used as a convex proxy to restrict the rank of $Z_{\mathbf{k}}$ (Fazel 2002, Recht et al. 2010).

The convexity of the objective function and the linearity of the constraint set in CC imply the existence of a unique globally optimal solution $(X_{\mathbf{k}}^*, Z_{\mathbf{k}}^*)$. This solution reproduces all available entries of the stationary covariance matrix $V_{\mathbf{k}}^{\text{dns}}$ resulting from DNS (or experiments) and completes unavailable second-order statistics via low-complexity stochastic dynamical model given by Equation 11. In particular, the factorization of $Z_{\mathbf{k}}^*$ can be used to determine $B_{\mathbf{k}}^*$ and $H_{\mathbf{k}}^*$, which along with $X_{\mathbf{k}}^*$ yield a low-rank modification $B_{\mathbf{k}}^* K_{\mathbf{k}}^*$ to $A_{\mathbf{k}}$ in Equation 11. This approach provides a *model which refines predictive power of the linearized NS equations by employing data while preserving relevant physics of turbulent flows*.

Figure 12 shows covariance matrices $V_{\mathbf{k},uu}$ and $V_{\mathbf{k},uv}$ resulting from DNS of turbulent channel flow with $Re = 186$ (left plots) and the solution to optimization problem CC with $\gamma = 300$ (right plots) for $\mathbf{k} = (2.5, 7)$. Black lines along the main diagonals mark the one-point correlations (in y) that are used as *available data* in CC and are *perfectly matched*. Using a Frobenius norm measure, $\|V_{\mathbf{k}}^* - V_{\mathbf{k}}^{\text{dns}}\|_F / \|V_{\mathbf{k}}^{\text{dns}}\|_F$, approximately 60% of $V_{\mathbf{k}}^{\text{dns}}$ can be recovered by the stationary covariance matrix $V_{\mathbf{k}}^* = C_{\mathbf{k}} X_{\mathbf{k}}^* C_{\mathbf{k}}^*$ of velocity fluctuations resulting from the solution of problem CC (Zare et al. 2017b). The high-quality recovery of two-point correlations is attributed to the Lyapunov-like structural constraint in CC, which *keeps physics in the mix and enforces consistency between data and the linearized dynamics*.

Alternative formulations. Covariance completion problem CC can be cast as an optimal control problem aimed at establishing a trade-off between control energy and the number of feedback couplings that are required to modify $A_{\mathbf{k}}$ in System 11 and achieve consistency with available data (Zare et al. 2019, 2020). Depending on modeling purpose and available data, many alternative turbulence modeling formulations are possible. Jovanović & Bamieh (2001) showed that portions of one-point correlations in (x, y, z) , resulting from the integration of DNS-based $V_{\mathbf{k}}^{\text{ker}}(y, y)$ over \mathbf{k} , can be approximated by the appropriate choice of covariance of white-in-time forcing to the NS equations linearized around turbulent mean velocity. This early success inspired the development of optimization algorithms for approximation of full covariance matrices using stochastic dynamical models (Hoepffner 2005, Lin & Jovanović 2009). For the eddy-viscosity enhanced linearization, Moarref & Jovanović (2012) demonstrated that white-in-time forcing with variance proportional to the turbulent energy spectrum can be used to reproduce the DNS-based energy spectrum of velocity fluctuations. Hwang & Eckhardt (2020) determined the wave-number dependence of the variance of stochastic forcing, which is uncorrelated in t and y , that minimizes the difference between the Reynolds shear stresses resulting from the mean and the linearized eddy-viscosity enhanced NS equations. Several recent efforts were aimed at matching individual entries of the spectral density matrix $S_{\mathbf{k}}(i\omega)$ at given frequencies (Beneddine et al. 2016, 2017, Towne et al. 2020) or at capturing the spectral power, $\text{trace}(S_{\mathbf{k}}(i\omega))$, (Morra et al. 2019). Finally, compared to the standard resolvent analysis (Moarref et al. 2014), an optimization-based approach that utilizes a componentwise approach (Rosenberg & McKeon 2019) offers con-

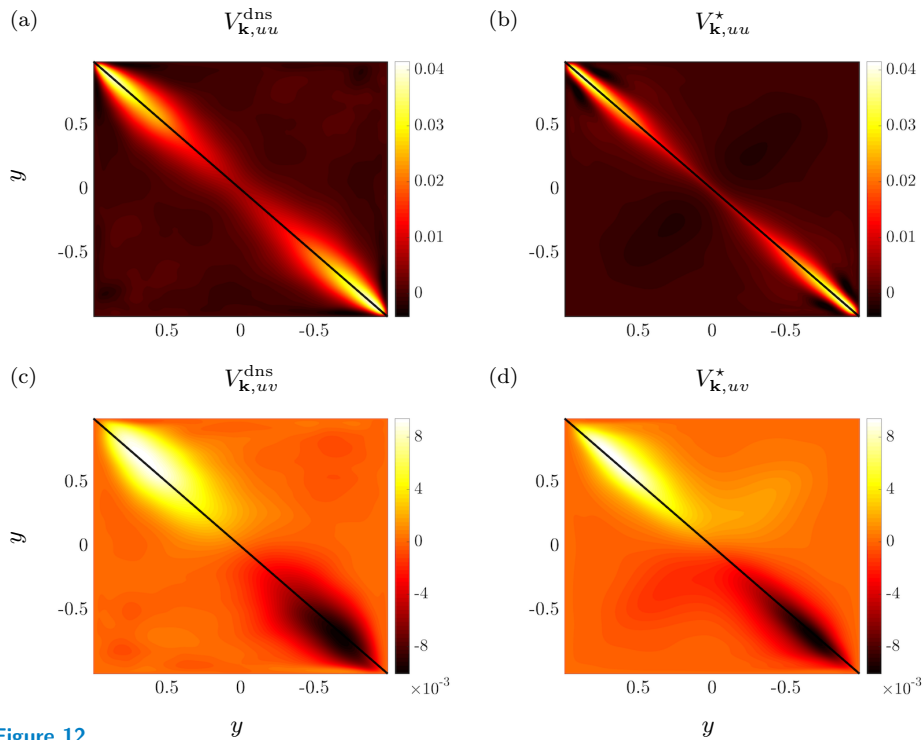


Figure 12

(a, b) Streamwise $V_{\mathbf{k},uu}$ and (c,d) streamwise/wall-normal $V_{\mathbf{k},uv}$ covariance matrices resulting from DNS of turbulent channel flow with $Re = 186$ (left plots); and the solution to optimization problem CC with $\gamma = 300$ (right plots) for $\mathbf{k} = (2.5, 7)$. Black lines along the main diagonals mark the one-point correlations that are used as available data in CC and are perfectly matched.

siderable improvement in matching spectra and co-spectra in turbulent channel flow (McMullen et al. 2020). This further exemplifies the power and versatility of the componentwise input-output viewpoint of fluid flows that was introduced in Jovanović & Bamieh (2005).

SUMMARY POINTS

1. The following quote is attributed to Eric Eady: “*It is not the process of linearization that limits insight. It is the nature of the state that we choose to linearize about.*” In addition, this review demonstrates that *the tools that we use to study the linearized equations are as important as the base flow that we choose to linearize about.*
2. Componentwise input-output analysis *uncovers mechanisms* for subcritical transition and identifies streamwise streaks, oblique waves, and Orr-Sommerfeld modes as input-output resonances from forcing to velocity components.
3. Input-output analysis *discovers a viscoelastic analogue of the familiar inertial lift-up mechanism.* This mechanism arises from stretching of polymer stress fluctuations by a base shear and, even in the absence of inertia, it induces significant amplification that can trigger transition to elastic turbulence in rectilinear flows.
4. Input-output analysis *quantifies impact of forcing and energy-content of velocity components.* It reveals influence of dimensionless groups (e.g., Reynolds and Weis-

senberg numbers) on amplification of deterministic and stochastic disturbances and identifies relevant spatio-temporal scales as well as the dominant flow structures.

5. Input-output viewpoint provides a *model-based approach to vibrational flow control*, where the dynamics are impacted by zero-mean oscillations. Effective strategies for controlling the onset of turbulence and turbulence suppression can be designed by examining the dynamics of fluctuations around the base flow induced by oscillations.
6. Linearized NS equations with stochastic forcing qualitatively predict structural features of turbulent shear flows and provide sufficient flexibility to *account for two-point correlations of fully-developed turbulence via low-complexity models*.
7. Input-output framework provides a *data-driven refinement of a physics-based model*, guarantees statistical consistency, and captures complex dynamics of turbulent flows in a way that is tractable for analysis, optimization, and control design.
8. Tools and ideas from control theory and convex optimization overcome shortcomings of physics-agnostic machine learning algorithms and enable the development of *theory and techniques for physics-aware data-driven turbulence modeling*.

FUTURE ISSUES

1. **Complex fluids and complex flows.** Among other emerging applications, input-output analysis is expected to clarify the importance of different physical mechanisms in the presence of surface roughness and free-stream disturbances, and to quantify the impact of modeling uncertainties that arise from chemical reactions and gas surface interactions in hypersonic flows (Candler 2019).
2. **Computational complexity.** For an evolution model with n degrees of freedom, the tools presented in this review require $O(n^3)$ computations. Such computations are routine for canonical flows, but the large-scale nature of spatially-discretized models in complex geometries induces significant computational overhead.
3. **Nonlinear interactions.** Precise characterization of the interplay between high flow sensitivity and nonlinearity in order to capture later stages of disturbance development, identify possible routes for transition, and design effective control strategies for the nonlinear NS equations remains a grand challenge.
4. **Data-driven techniques.** In spite of the apparent promise of machine and reinforcement learning, a number of challenges have to be addressed, including the development of methods that respect physical constraints, generalize to flow regimes that are not accounted for in the available data, and offer convergence, performance, and robustness guarantees on par with model-based approaches to flow control.
5. **Feedback control.** A host of challenges including estimation using noisy measurements, optimal sensor and actuator placement, efficient computation of optimal and robust controllers, structured and distributed control synthesis, as well as convergence and sample complexity of data-driven reinforcement learning strategies have to be addressed to enable a successful feedback control at high Reynolds numbers.

6. DISCUSSION

Herein, we expand on future issues and provide an overview of outstanding challenges.

Complex fluids and complex flows. In addition to parallel flows, input-output analysis was utilized to quantify the influence of deterministic (Sipp & Marquet 2013) and stochastic (Ran et al. 2019) inputs as well as base flow variations (Brandt et al. 2011) on spatially-evolving boundary layers. In high-speed compressible flows, there is a coupling of inertial and thermal effects, and experiments suggest a significant impact of exogenous disturbances on transition (Fedorov 2011). Traditional receptivity is based on a local spatial analysis (Malik 1989, Bertolotti & Herbert 1991), and is not applicable to most bodies of aerodynamic interest. For hypersonic vehicles with complex geometry or shock interactions with control surfaces, transition is poorly understood, and empirical testing is typically used to characterize their behavior. Linearization around spatially-evolving base flows in the presence of sharp gradients involves multiple inhomogeneous directions, and even modal stability analysis becomes challenging and computationally demanding (Hildebrand et al. 2018, Sidharth et al. 2018). Recently, Dwivedi et al. (2019) employed a global input-output analysis to quantify the amplification of exogenous disturbances and explain the appearance of experimentally observed steady reattachment streaks in a hypersonic flow over a compression ramp. For the laminar shock-boundary layer interaction, this study showed that upstream counter-rotating vortices trigger streaks with a preferential spanwise length scale. Input-output analysis is expected to clarify the importance of different physical mechanisms in the presence of surface roughness and free-stream disturbances, and to quantify the impact of modeling uncertainties that arise from chemical reactions and gas surface interactions on hypersonic flows (Candler 2019).

Computational complexity. For an evolution model with n degrees of freedom, the tools presented in this review require $O(n^3)$ computations. Such computations are routine for canonical flows, but the large-scale nature of spatially-discretized models in complex geometries induces significant computational overhead. Dominant singular values of the state-transition and frequency response operators can be computed iteratively (Schmid 2007) or via randomized techniques (Halko et al. 2011). Such computations have been used to conduct nonmodal analysis of complex flows (Jeun et al. 2016, Dwivedi et al. 2019). While in general it is challenging to efficiently solve large-scale Lyapunov equations, efficient iterative algorithms (both in terms of memory and computations) exist for systems with a small number of inputs and outputs and sparse dynamic matrices (Benner et al. 2008). These are expected to bring the utility of stochastic analysis from canonical channels (Jovanović & Bamieh 2005) and boundary layers (Ran et al. 2019) to flows in complex geometries.

Nonlinear interactions. Large amplification of disturbances in conjunction with nonlinear interactions can induce secondary instability of streamwise streaks, their breakdown, and transition (Waleffe 1997). An alternative self-sustaining mechanism shows that turbulence can be triggered by the streamwise-constant NS equations in feedback with a stochastically-forced streamwise-varying linearization (Farrell & Ioannou 2012, Thomas et al. 2014). Nonlinear nonmodal stability analysis identifies initial conditions of a given amplitude that maximize energy at a fixed time (Kerswell 2018). Dissipation inequalities (Ahmadi et al. 2019) and a harmonic balance approach (Rigas et al. 2020) were recently utilized to extend input-output analysis to the nonlinear NS equations, and the theory of integral quadratic constraints (Megretski & Rantzer 1997) was used to study of a phenomenological model of transition (Kalur et al. 2020). However, it is still an open challenge to precisely characterize the interplay between high flow sensitivity and nonlinearity in order to capture later stages

of transition routes and design effective control strategies.

Data-driven techniques. Machine learning has revolutionized many disciplines, e.g., image recognition and speech processing, and is increasingly used in modeling and decision making based on available data. While the NS equations are often too complex for model-based optimization and control, DNS provides data for reduced-order dynamical modeling (Rowley 2005, Lumley 2007, Schmid 2010, Jovanović et al. 2014, Towne et al. 2018). Capitalizing on the availability of such data, machine and reinforcement learning have recently been used for flow modeling, optimization, and control (Brunton et al. 2020) and this trend will continue. In spite of the apparent promise, a number of challenges have to be addressed, including the development of methods that respect physical constraints, generalize to flow regimes that were not accounted for in the available data sets, and offer convergence, performance, and robustness guarantees on par with model-based approaches to flow control.

Feedback control offers a more viable approach than sensor-less control for dealing with uncertainties that impact the operation of engineering flows. The scale and complexity of the problem introduce significant challenges for modeling, sensor and actuator placement, and control design. These necessitate the development of model-based and data-driven techniques. In wall-bounded flows at low Reynolds numbers, model-based feedback control has shown significant promise (Joshi et al. 1997, Bewley & Liu 1998, Högberg et al. 2003a,b, Kim & Bewley 2007). Since sensing and actuation are typically restricted to the surface, the flow field needs to be estimated using limited noisy measurements in order to form a control action. Hoepffner et al. (2005), Chevalier et al. (2006) demonstrated the importance of statistics of disturbances in the design of estimation gains. Alternatively, the data-refined model, given by Equation 11, that matches statistics of turbulent flows can be readily embedded into a Kalman filter estimation framework. Alongside estimation, challenges associated with the optimal sensor and actuator placement (Chen & Rowley 2011, Zare et al. 2019), efficient computation of optimal and robust controllers (Bewley et al. 2016), structured and distributed control synthesis (Lin et al. 2013), as well as convergence and sample complexity of data-driven reinforcement learning strategies (Mohammadi et al. 2019) have to be addressed to enable a successful feedback control at high Reynolds numbers.

DISCLOSURE STATEMENT

The author is not aware of any affiliations, memberships, funding, or financial holdings that might be perceived as affecting the objectivity of this review.

ACKNOWLEDGMENTS

I would like to thank Bassam Bamieh for his mentorship, friendship, and support over the years. Bassam inspired me to work at the interface between fluid mechanics and control and has been an intellectual role model for me from the first day we met. I am grateful to Parviz Moin for welcoming me to the Center for Turbulence Research at Stanford University on numerous occasions; these visits pushed me out of my comfort zone and made me a better researcher. I am indebted to Makan Fardad, Tryphon Georgiou, Satish Kumar, Joe Nichols, and Peter Schmid for our collaborations and for their thoughtful feedback about this review; we enjoy spending time with each other and our scientific interactions are a consequence of our friendship. This work would not have been possible without contributions of my current and former PhD students Anubhav Dwivedi, Gokul Hariharan, Nazish Hoda, Binh Lieu, Fu Lin, Rashad Moarref, Wei Ran, and Armin Zare and without support from the Air Force Office of Scientific Research under Awards FA9550-16-1-0009 and FA9550-18-1-0422, and from the National Science Foundation under Award ECCS-1809833.

LITERATURE CITED

- Agarwal A, Brandt L, Zaki TA. 2014. Linear and nonlinear evolution of a localized disturbance in polymeric channel flow. *J. Fluid Mech.* 760:278–303
- Ahmadi M, Valmorbida G, Gayme D, Papachristodoulou A. 2019. A framework for input-output analysis of wall-bounded shear flows. *J. Fluid Mech.* 873:742–785
- Bamieh B, Dahleh M. 2001. Energy amplification in channel flows with stochastic excitation. *Phys. Fluids* 13:3258–3269**
- Bandyopadhyay PR. 2006. Stokes mechanism of drag reduction. *J. Appl. Mech.* 73:483
- Beneddine S, Sipp D, Arnault A, Dandois J, Lesshafft L. 2016. Conditions for validity of mean flow stability analysis. *J. Fluid Mech.* 798:485–504
- Beneddine S, Yegavian R, Sipp D, Leclaire B. 2017. Unsteady flow dynamics reconstruction from mean flow and point sensors: an experimental study. *J. Fluid Mech.* 824:174–201
- Benner P, Li JR, Penzl T. 2008. Numerical solution of large-scale Lyapunov equations, Riccati equations, and linear-quadratic optimal control problems. *Numer. Linear Algebra Appl.* 15:755–777
- Bertolotti FP, Herbert T. 1991. Analysis of the linear stability of compressible boundary layers using the PSE. *Theoret. Comput. Fluid Dyn.* 3:117–124
- Bewley T, Luchini P, Pralits J. 2016. Methods for solution of large optimal control problems that bypass open-loop model reduction. *Meccanica* 51:2997–3014
- Bewley TR. 2009. A fundamental limit on the balance of power in a transpiration-controlled channel flow. *J. Fluid Mech.* 632:443–446
- Bewley TR, Liu S. 1998. Optimal and robust control and estimation of linear paths to transition. *J. Fluid Mech.* 365:305–349
- Bird RB, Curtiss CF, Armstrong RC, Hassager O. 1987. Dynamics of Polymeric Liquids. Wiley
- Boyd S, Vandenberghe L. 2004. Convex optimization. Cambridge University Press
- Brandt L, Sipp D, Pralits JO, Marquet O. 2011. Effect of base-flow variation in noise amplifiers: the flat-plate boundary layer. *J. Fluid Mech.* 687:503–528
- Brunton SL, Noack BR, Koumoutsakos P. 2020. Machine learning for fluid mechanics. *Annu. Rev. Fluid Mech.* 52:477–508
- Butler KM, Farrell BF. 1992. Three-dimensional optimal perturbations in viscous shear flow. *Phys. Fluids A* 4:1637**
- Butler KM, Farrell BF. 1993. Optimal perturbations and streak spacing in wall-bounded turbulent shear flow. *Phys. Fluids A* 5:774–777
- Candler GV. 2019. Rate effects in hypersonic flows. *Annu. Rev. of Fluid Mech.* 51:379–402
- Chavarin A, Luhar M. 2020. Resolvent analysis for turbulent channel flow with riblets. *AIAA Journal* 58:589–599
- Chen KK, Rowley CW. 2011. H_2 optimal actuator and sensor placement in the linearised complex Ginzburg-Landau system. *J. Fluid Mech.* 681:241–260
- Chevalier M, Hoepffner J, Bewley TR, Henningson DS. 2006. State estimation in wall-bounded flow systems. Part 2. Turbulent flows. *J. Fluid Mech.* 552:167–187
- Choi KS. 2002. Near-wall structure of turbulent boundary layer with spanwise-wall oscillation. *Phys. Fluids* 14:2530–2542
- Choi KS, DeBisschop JR, Clayton BR. 1998. Turbulent boundary-layer control by means of spanwise-wall oscillation. *AIAA J.* 36:1157–1163
- Cossu C, Pujals G, Depardon S. 2009. Optimal transient growth and very large-scale structures in turbulent boundary layers. *J. Fluid Mech.* 619:79–94
- del Álamo JC, Jiménez J. 2003. Spectra of the very large anisotropic scales in turbulent channels. *Phys. Fluids* 15:41–44

Reynolds number
scaling of energy
amplification

Transient growth
analysis of
transition

Transient growth analysis of eddy-viscosity enhanced linearized NS equations

Input-output analysis of hypersonic flow

First use of the linearized NS equations with stochastic forcing to study transition

Input-output analysis of viscoelastic fluids

- del Álamo JC, Jiménez J. 2006. Linear energy amplification in turbulent channels. *J. Fluid Mech.* 559:205–213
- del Álamo JC, Jiménez J, Zandonade P, Moser RD. 2004. Scaling of the energy spectra of turbulent channels. *J. Fluid Mech.* 500:135–144
- Dhanak M, Si C. 1999. On reduction of turbulent wall friction through spanwise wall oscillations. *J. Fluid Mech.* 383:175–195
- Duraisamy K, Iaccarino G, Xiao H. 2019. Turbulence modeling in the age of data. *Annu. Rev. Fluid Mech.* 51:357–377
- Dwivedi A, Sidharth GS, Nichols JW, Candler GV, Jovanović MR. 2019. Reattachment vortices in hypersonic compression ramp flow: an input-output analysis. *J. Fluid Mech.* 880:113–135
- Farrell BF, Ioannou PJ. 1993. Stochastic forcing of the linearized Navier-Stokes equations. *Phys. Fluids A* 5:2600–2609
- Farrell BF, Ioannou PJ. 2012. Dynamics of streamwise rolls and streaks in turbulent wall-bounded shear flow. *J. Fluid Mech.* 708:149–196
- Fazel M. 2002. Matrix rank minimization with applications. Ph.D. thesis, Stanford University
- Fedorov A. 2011. Transition and stability of high-speed boundary layers. *Annu. Rev. of Fluid Mech.* 43:79–95
- Fransson JHM, Talamelli A, Brandt L, Cossu C. 2006. Delaying transition to turbulence by a passive mechanism. *Phys. Rev. Lett.* 96:064501
- Fukagata K, Sugiyama K, Kasagi N. 2009. On the lower bound of net driving power in controlled duct flows. *Physica D: Nonlinear Phenomena* 238:1082–1086
- Gardner W. 1990. Introduction to Random Processes: with Applications to Signals and Systems. McGraw-Hill
- Garnaud X, Sandberg RD, Lesshafft L. 2013. Global response to forcing in a subsonic jet: instability wavepackets and acoustic radiation, In *19th AIAA/CEAS Aeroacoustics Conference*, p. 2232
- Georgiou TT. 2002a. Spectral analysis based on the state covariance: the maximum entropy spectrum and linear fractional parametrization. *IEEE Trans. Autom. Control* 47:1811–1823
- Georgiou TT. 2002b. The structure of state covariances and its relation to the power spectrum of the input. *IEEE Trans. Autom. Control* 47:1056–1066
- Groisman A, Steinberg V. 2000. Elastic turbulence in a polymer solution flow. *Nature* 405:53–55
- Gustavsson LH. 1991. Energy growth of three-dimensional disturbances in plane Poiseuille flow. *J. Fluid Mech.* 98:149
- Halko N, Martinsson PG, Tropp JA. 2011. Finding structure with randomness: Probabilistic algorithms for constructing approximate matrix decompositions. *SIAM Rev.* 53:217–288
- Hariharan G, Jovanović MR, Kumar S. 2018. Amplification of localized body forces in channel flows of viscoelastic fluids. *J. Non-Newtonian Fluid Mech.* 260:40–53
- Hildebrand N, Dwivedi A, Nichols JW, Jovanović MR, Candler GV. 2018. Simulation and stability analysis of oblique shock wave/boundary layer interactions at Mach 5.92. *Phys. Rev. Fluids* 3:013906
- Hoda N, Jovanović MR, Kumar S. 2008. Energy amplification in channel flows of viscoelastic fluids. *J. Fluid Mech.* 601:407–424
- Hoda N, Jovanović MR, Kumar S. 2009. Frequency responses of streamwise-constant perturbations in channel flows of Oldroyd-B fluids. *J. Fluid Mech.* 625:411–434
- Hœpffner J. 2005. Modeling flow statistics using convex optimization, In *Proceedings of the 2005 European Control Conference and the 44th IEEE Conference on Decision and Control*, pp. 4287–4292
- Hœpffner J, Chevalier M, Bewley TR, Henningson DS. 2005. State estimation in wall-bounded flow

- systems. Part 1. Perturbed laminar flows. *J. Fluid Mech.* 534:263–294
- Hœpffner J, Fukagata K. 2009. Pumping or drag reduction? *J. Fluid Mech.* 635:171–187
- Högberg M, Bewley TR, Henningson DS. 2003a. Linear feedback control and estimation of transition in plane channel flow. *J. Fluid Mech.* 481:149–175
- Högberg M, Bewley TR, Henningson DS. 2003b. Relaminarization of $Re_\tau = 100$ turbulence using linear state-feedback control. *Phys. Fluids* 15:3572–3575
- Hwang Y, Cossu C. 2010a. Amplification of coherent streaks in the turbulent Couette flow: an input-output analysis at low Reynolds number. *J. Fluid Mech.* 643:333–348**
- Hwang Y, Cossu C. 2010b. Linear non-normal energy amplification of harmonic and stochastic forcing in the turbulent channel flow. *J. Fluid Mech.* 664:51–73**
- Hwang Y, Eckhardt B. 2020. Attached eddy model revisited using a minimal quasi-linear approximation. *J. Fluid Mech.* Submitted
- Jeun J, Nichols JW, Jovanović MR. 2016. Input-output analysis of high-speed axisymmetric isothermal jet noise. *Phys. Fluids* 28:047101**
- Jordan P, Colonius T. 2013. Wave packets and turbulent jet noise. *Annu. Rev. Fluid Mech.* 45:173–195
- Joshi SS, Speyer JL, Kim J. 1997. A systems theory approach to the feedback stabilization of infinitesimal and finite-amplitude disturbances in plane Poiseuille flow. *J. Fluid Mech.* 332:157–184
- Jovanović MR. 2004. Modeling, analysis, and control of spatially distributed systems. Ph.D. thesis, University of California, Santa Barbara
- Jovanović MR. 2008. Turbulence suppression in channel flows by small amplitude transverse wall oscillations. *Phys. Fluids* 20:014101
- Jovanović MR, Bamieh B. 2001. Modelling flow statistics using the linearized Navier-Stokes equations, In *Proceedings of the 40th IEEE Conference on Decision and Control*, pp. 4944–4949
- Jovanović MR, Bamieh B. 2005. Componentwise energy amplification in channel flows. *J. Fluid Mech.* 534:145–183**
- Jovanović MR, Fardad M. 2008. H_2 norm of linear time-periodic systems: a perturbation analysis. *Automatica* 44:2090–2098
- Jovanović MR, Georgiou TT. 2010. Reproducing second order statistics of turbulent flows using linearized Navier-Stokes equations with forcing, In *Bulletin of the American Physical Society*
- Jovanović MR, Kumar S. 2010. Transient growth without inertia. *Phys. Fluids* 22:023101**
- Jovanović MR, Kumar S. 2011. Nonmodal amplification of stochastic disturbances in strongly elastic channel flows. *J. Non-Newtonian Fluid Mech.* 166:755–778**
- Jovanović MR, Schmid PJ, Nichols JW. 2014. Sparsity-promoting dynamic mode decomposition. *Phys. Fluids* 26:024103
- Jung W, Mangiavacchi N, Akhavan R. 1992. Suppression of turbulence in wall-bounded flows by high-frequency spanwise oscillations. *Phys. Fluids A* 4:1605–1607
- Kalur A, Seiler PJ, Hemati M. 2020. Stability and performance analysis of nonlinear and non-normal systems using quadratic constraints, In *Proceedings of the 2020 AIAA SciTech Forum and Exposition*, p. 0833
- Kerswell RR. 2018. Nonlinear nonmodal stability theory. *Annu. Rev. Fluid Mech.* 50:319–345
- Kim J, Bewley TR. 2007. A linear systems approach to flow control. *Annu. Rev. Fluid Mech.* 39:383–417
- Kim J, Lim J. 2000. A linear process in wall-bounded turbulent shear flows. *Phys. Fluids* 12:1885–1888
- Kim J, Moin P, Moser R. 1987. Turbulence statistics in fully developed channel flow at low Reynolds number. *J. Fluid Mech.* 177:133–166

Input-output analysis of eddy-viscosity enhanced linearized NS equations

Input-output analysis of jet noise

Componentwise input-output analysis

Viscoelastic lift-up mechanism

Lift-up mechanism

- Kwakernaak H, Sivan R. 1972. Linear optimal control systems. Wiley-Interscience
- Laadhari F, Skandaji L, Morel R. 1994. Turbulence reduction in a boundary layer by a local spanwise oscillating surface. *Phys. Fluids* 6:3218–3220
- Landahl MT. 1975. Wave breakdown and turbulence. *SIAM J. Appl. Math.* 28:735–756**
- Larson RG, Shaqfeh ESG, Muller SJ. 1990. A purely elastic instability in Taylor-Couette flow. *J. Fluid Mech.* 218:573–600
- Lee C, Min T, Kim J. 2008. Stability of a channel flow subject to wall blowing and suction in the form of a traveling wave. *Phys. Fluids* 20:101513
- Lee MJ, Kim J, Moin P. 1990. Structure of turbulence at high shear rate. *J. Fluid Mech.* 216:561–583
- Lieu BK, Jovanović MR, Kumar S. 2013. Worst-case amplification of disturbances in inertialess Couette flow of viscoelastic fluids. *J. Fluid Mech.* 723:232–263
- Lieu BK, Moarref R, Jovanović MR. 2010. Controlling the onset of turbulence by streamwise traveling waves. Part 2: Direct numerical simulations. *J. Fluid Mech.* 663:100–119
- Lin F, Fardad M, Jovanović MR. 2013. Design of optimal sparse feedback gains via the alternating direction method of multipliers. *IEEE Trans. Automat. Control* 58:2426–2431
- Lin F, Jovanović MR. 2009. Least-squares approximation of structured covariances. *IEEE Trans. Automat. Control* 54:1643–1648
- Luhar M, Sharma AS, McKeon BJ. 2014. Opposition control within the resolvent analysis framework. *J. Fluid Mech.* 749:597–626
- Lumley JL. 2007. Stochastic tools in turbulence. Dover Publications
- Malik MR. 1989. Prediction and control of transition in supersonic and hypersonic boundary layers. *AIAA J.* 27:1487–1493
- Malkus WVR. 1956. Outline of a theory of turbulent shear flow. *J. Fluid Mech.* 1:521–539
- Marusic I, Joseph DD, Mahesh K. 2007. Laminar and turbulent comparisons for channel flow and flow control. *J. Fluid Mech.* 570:467–477
- McKeon BJ, Sharma AS. 2010. A critical-layer framework for turbulent pipe flow. *J. Fluid Mech.* 658:336–382**
- McMullen RM, Rosenberg K, McKeon BJ. 2020. Interaction of forced Orr-Sommerfeld and Squire modes in a low-order representation of turbulent channel flow. arXiv:2001.02785
- Megretski A, Rantzer A. 1997. System analysis via integral quadratic constraints. *IEEE Trans. Autom. Control* 42:819–830
- Min T, Kang SM, Speyer JL, Kim J. 2006. Sustained sub-laminar drag in a fully developed channel flow. *J. Fluid Mech.* 558:309–318**
- Moarref R, Jovanović MR. 2010. Controlling the onset of turbulence by streamwise traveling waves. Part 1: Receptivity analysis. *J. Fluid Mech.* 663:70–99**
- Moarref R, Jovanović MR. 2012. Model-based design of transverse wall oscillations for turbulent drag reduction. *J. Fluid Mech.* 707:205–240**
- Moarref R, Jovanović MR, Tropp JA, Sharma AS, McKeon BJ. 2014. A low-order decomposition of turbulent channel flow via resolvent analysis and convex optimization. *Phys. Fluids* 26:051701
- Moarref R, Sharma AS, Tropp JA, McKeon BJ. 2013. Model-based scaling of the streamwise energy density in high-Reynolds-number turbulent channels. *J. Fluid Mech.* 734:275–316
- Mohammadi H, Zare A, Soltanolkotabi M, Jovanović MR. 2019. Convergence and sample complexity of gradient methods for the model-free linear quadratic regulator problem. *IEEE Trans. Automat. Control* Submitted; also arXiv:1912.11899
- Moin P, Moser RD. 1989. Characteristic-eddy decomposition of turbulence in a channel. *J. Fluid Mech.* 200:471–509
- Morra P, Semeraro O, Henningson DS, Cossu C. 2019. On the relevance of Reynolds stresses in resolvent analyses of turbulent wall-bounded flows. *J. Fluid Mech.* 867:969–984

Resolvent analysis of turbulent flow

Sub-laminar drag via traveling waves

Model-based design of traveling waves

Model-based design of wall-oscillations

- Noack BR, Morzyński M, Tadmor G. 2011. Reduced-order modelling for flow control, vol. 528 of *CISM Courses and Lectures*. Springer
- Odeh F, Keller JB. 1964. Partial differential equations with periodic coefficients and Bloch waves in crystals. *J. Math. Phys.* 5:1499–1504
- Page J, Zaki TA. 2014. Streak evolution in viscoelastic Couette flow. *J. Fluid Mech.* 742:520–551
- Pope SB. 2000. Turbulent flows. Cambridge University Press
- Pujals G, García-Villalba M, Cossu C, Depardon S. 2009. A note on optimal transient growth in turbulent channel flows. *Phys. Fluids* 21:015109
- Qin B, Salipante PF, Hudson SD, Arratia PE. 2019a. Flow resistance and structures in viscoelastic channel flows at low Re . *Phys. Rev. Lett.* 123:194501
- Qin B, Salipante PF, Hudson SD, Arratia PE. 2019b. Upstream vortex and elastic wave in the viscoelastic flow around a confined cylinder. *J. Fluid Mech.* 864:R2
- Quadrio M, Ricco P. 2004. Critical assessment of turbulent drag reduction through spanwise wall oscillations. *J. Fluid Mech.* 521:251–271
- Ran W, Zare A, Hack MJP, Jovanović MR. 2019. Stochastic receptivity analysis of boundary layer flow. *Phys. Rev. Fluids* 4:093901**
- Ran W, Zare A, Jovanović MR. 2020. Model-based design of riblets for turbulent drag reduction. *J. Fluid Mech.* Submitted; also arXiv:2002.01671
- Recht B, Fazel M, Parrilo PA. 2010. Guaranteed minimum-rank solutions of linear matrix equations via nuclear norm minimization. *SIAM Rev.* 52:471–501
- Reynolds WC, Hussain AKMF. 1972. The mechanics of an organized wave in turbulent shear flow. Part 3. Theoretical models and comparisons with experiments. *J. Fluid Mech.* 54:263–288
- Reynolds WC, Tiederman WG. 1967. Stability of turbulent channel flow with application to Malkus’s theory. *J. Fluid Mech.* 27:253–272
- Ricco P. 2004. Modification of near-wall turbulence due to spanwise wall oscillations. *J. Turbul.*
- Ricco P. 2011. Laminar streaks with spanwise wall forcing. *Phys. Fluids* 23:064103
- Ricco P, Quadrio M. 2008. Wall-oscillation conditions for drag reduction in turbulent channel flow. *International Journal of Heat and Fluid Flow* 29:891–902
- Rigas G, Sipp D, Colonius T. 2020. Non-linear input/output analysis: application to boundary layer transition. arXiv:2001.09440
- Rosenberg K, McKeon BJ. 2019. Efficient representation of exact coherent states of the Navier-Stokes equations using resolvent analysis. *Fluid Dyn. Res.* 51:011401
- Rowley CW. 2005. Model reduction for fluids using balanced proper orthogonal decomposition. *Intl J. Bifurcation Chaos* 15:997–1013
- Rowley CW, Dawson ST. 2017. Model reduction for flow analysis and control. *Annu. Rev. Fluid Mech.* 49:387–417
- Schmid PJ. 2007. Nonmodal stability theory. *Annu. Rev. Fluid Mech.* 39:129–162
- Schmid PJ. 2010. Dynamic mode decomposition of numerical and experimental data. *J. Fluid Mech.* 656:5–28
- Schmid PJ, Henningson DS. 2001. Stability and transition in shear flows. New York: Springer-Verlag
- Sidharth G, Dwivedi A, Candler GV, Nichols JW. 2018. Onset of three-dimensionality in supersonic flow over a slender double wedge. *Physical Rev. Fluids* 3:093901
- Sipp D, Marquet O. 2013. Characterization of noise amplifiers with global singular modes: the case of the leading-edge flat-plate boundary layer. *Theor. Comp. Fluid Dyn.* 27:617–635**
- Tadmor G, Noack BR. 2011. Bernoulli, Bode, and Budgie [Ask the Experts]. *IEEE Contr. Syst. Mag.* 31:18–23
- Thomas VL, Lieu BK, Jovanović MR, Farrell BF, Ioannou PJ, Gayme DF. 2014. Self-sustaining turbulence in a restricted nonlinear model of plane Couette flow. *Phys. Fluids* 26:105112
- Toedtli SS, Luhar M, McKeon BJ. 2019. Predicting the response of turbulent channel flow to

Input-output
analysis of
boundary layer
with stochastic
forcing

Input-output
analysis of
boundary layer

varying-phase opposition control: Resolvent analysis as a tool for flow control design. *Phys. Rev. Fluids* 4:073905

Towne A, Lozano-Durán A, Yang X. 2020. Resolvent-based estimation of space-time flow statistics. *J. Fluid Mech.* 883:A17

Towne A, Schmidt OT, Colonius T. 2018. Spectral proper orthogonal decomposition and its relationship to dynamic mode decomposition and resolvent analysis. *J. Fluid Mech.* 847:821–867

Trefethen LN, Embree M. 2005. Spectra and pseudospectra: the behavior of nonnormal matrices and operators. Princeton: Princeton University Press

Trefethen LN, Trefethen AE, Reddy SC, Driscoll TA. 1993. Hydrodynamic stability without eigenvalues. *Science* 261:578–584

Waleffe F. 1997. On a self-sustaining process in shear flows. *Phys. Fluids* 9:883–900

Weideman JAC, Reddy SC. 2000. A MATLAB differentiation matrix suite. *ACM Trans. Math. Software* 26:465–519

Zare A, Chen Y, Jovanović MR, Georgiou TT. 2017a. Low-complexity modeling of partially available second-order statistics: theory and an efficient matrix completion algorithm. *IEEE Trans. Automat. Control* 62:1368–1383

Zare A, Georgiou TT, Jovanović MR. 2020. Stochastic dynamical modeling of turbulent flows. *Annu. Rev. Control Robot. Auton. Syst.* 3. In press; doi:10.1146/annurev-control-053018-023843

Zare A, Jovanović MR, Georgiou TT. 2017b. Colour of turbulence. *J. Fluid Mech.* 812:636–680

Zare A, Mohammadi H, Dhingra NK, Georgiou TT, Jovanović MR. 2019. Proximal algorithms for large-scale statistical modeling and sensor/actuator selection. *IEEE Trans. Automat. Control* Doi:10.1109/TAC.2019.2948268; also arXiv:1807.01739

Zhou K, Doyle JC, Glover K. 1996. Robust and optimal control. Prentice Hall

Must-read. First use of resolvent analysis and pseudo-spectra in fluid mechanics

Self-sustaining mechanism

Turbulence modeling using the linearized NS equations with stochastic forcing
